(12) INTERNATIONAL APPLICATION PUBLISHED UNDER THE PATENT COOPERATION TREATY (PCT)

(19) World Intellectual Property Organization
International Bureau

(43) International Publication Date
14 March 2019 (14.03.2019)

WIPO | PCT

(10) International Publication Number
WO 2019/051305 A1

(51) International Patent Classification:
H01M 10/0562 (2010.01) *H01M 10/052* (2010.01)

(21) International Application Number:
PCT/US2018/050069

(22) International Filing Date:
07 September 2018 (07.09.2018)

(25) Filing Language: English

(26) Publication Language: English

(30) Priority Data:
62/556,045 08 September 2017 (08.09.2017) US

(71) Applicants: **THE BOARD OF TRUSTEES OF THE LELAND STANFORD JUNIOR UNIVERSITY** [US/US]; Office of the General Counsel, Building 170, Third Floor, Main Quad, P.O. Box 20386, Stanford, California 94305-2038 (US). **SOLID POWER, INC.** [US/US]; 486 S. Pierce Ave., Unit E, Louisville, Colorado 80027 (US).

(72) Inventors; and

(71) Applicants: **BUETTNER-GARRETT, Joshua** [US/US]; c/o Solid Power, Inc., 486 S. Pierce Ave., Unit E, Louisville, Colorado 80027 (US). **FRANCISCO, Brian E.** [US/US]; c/o Solid Power, Inc., 486 S. Pierce Ave., Unit E, Louisville, Colorado 80027 (US).

(72) Inventors: **SENDEK, Austin D.**; c/o The Board of Trustees of the Leland Stanford Junior University, Office of the General Counsel, Building 170, Third Floor, Main Quad, P.O. Box 20386, Stanford, California 94305-2038 (US). **CUBUK, Ekin D.**; c/o The Board of Trustees of the Leland Stanford Junior University, Office of the General Counsel, Building 170, Third Floor, Main Quad, P.O. Box 20386, Stanford, California 94305-2038 (US). **REED, Evan J.**; c/o The Board of Trustees of the Leland Stanford Junior University, Office of the General Counsel, Building 170, Third Floor, Main Quad, P.O. Box 20386, Stanford, California 94305-2038 (US).

(54) Title: CERAMIC MATERIAL WITH HIGH LITHIUM ION CONDUCTIVITY AND HIGH ELECTROCHEMICAL STABILITY FOR USE AS SOLID-STATE ELECTROLYTE AND ELECTRODE ADDITIVE

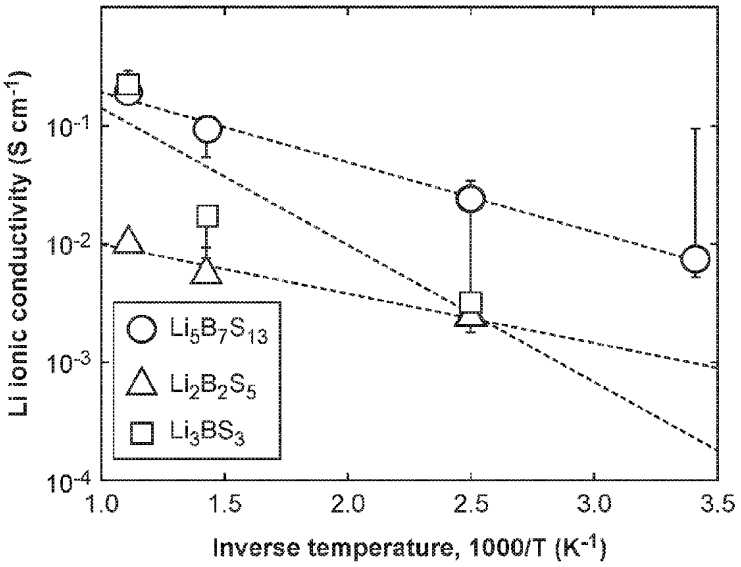

FIG. 1

(57) Abstract: A battery includes: (1) a cathode; (2) an anode; and (3) a solid-state electrolyte disposed between the cathode and the anode. At least one of the cathode, the anode, or the solid-state electrolyte includes a ceramic material including lithium (Li), boron (B), and sulfur (S), the ceramic material includes multiple crystalline phases and has an overall composition given by *a:b:c* molar ratio of Li:B:S, and *c/b* is in a range of about 1 to about 3.

WO 2019/051305 A1

[Continued on next page]

(74) **Agent: LIU, Cliff Z.** et al.; FOLEY & LARDNER LLP, 3000 K Street N.W., Suite 600, Washington, District of Columbia 20007-5109 (US).

(81) **Designated States** *(unless otherwise indicated, for every kind of national protection available)*: AE, AG, AL, AM, AO, AT, AU, AZ, BA, BB, BG, BH, BN, BR, BW, BY, BZ, CA, CH, CL, CN, CO, CR, CU, CZ, DE, DJ, DK, DM, DO, DZ, EC, EE, EG, ES, FI, GB, GD, GE, GH, GM, GT, HN, HR, HU, ID, IL, IN, IR, IS, JO, JP, KE, KG, KH, KN, KP, KR, KW, KZ, LA, LC, LK, LR, LS, LU, LY, MA, MD, ME, MG, MK, MN, MW, MX, MY, MZ, NA, NG, NI, NO, NZ, OM, PA, PE, PG, PH, PL, PT, QA, RO, RS, RU, RW, SA, SC, SD, SE, SG, SK, SL, SM, ST, SV, SY, TH, TJ, TM, TN, TR, TT, TZ, UA, UG, US, UZ, VC, VN, ZA, ZM, ZW.

(84) **Designated States** *(unless otherwise indicated, for every kind of regional protection available)*: ARIPO (BW, GH, GM, KE, LR, LS, MW, MZ, NA, RW, SD, SL, ST, SZ, TZ, UG, ZM, ZW), Eurasian (AM, AZ, BY, KG, KZ, RU, TJ, TM), European (AL, AT, BE, BG, CH, CY, CZ, DE, DK, EE, ES, FI, FR, GB, GR, HR, HU, IE, IS, IT, LT, LU, LV, MC, MK, MT, NL, NO, PL, PT, RO, RS, SE, SI, SK, SM, TR), OAPI (BF, BJ, CF, CG, CI, CM, GA, GN, GQ, GW, KM, ML, MR, NE, SN, TD, TG).

Published:

— *with international search report (Art. 21(3))*

CERAMIC MATERIAL WITH HIGH LITHIUM ION CONDUCTIVITY AND HIGH ELECTROCHEMICAL STABILITY FOR USE AS SOLID-STATE ELECTROLYTE AND ELECTRODE ADDITIVE

Cross-Reference to Related Application

[0001] This application claims the benefit of U.S. Provisional Application No. 62/556,045, filed September 8, 2017, the contents of which are incorporated herein by reference in their entirety.

Background

[0002] A discovery strategy for solid electrolyte materials is to search a chemical space for a material that simultaneously possesses fast ionic conduction and a wide electrochemical stability window. This strategy is guided by the empirical observation that electrolytes with an electrochemical stability window narrower than a potential difference across electrodes can undergo degradation reactions at electrode-electrolyte interfaces (EEIs) that result in interfacial products with poor ionic conductivity. These interfacial phases then block ionic motion between the electrodes and halt battery operation. Typically, degradation passivates the electrode against further reaction, but degradation can continue until an entire electrolyte reacts if one or more of the EEI degradation products are electron conductors.

[0003] Currently, the material LGPS ($Li_{10}GeP_2S_{12}$) is considered among the best available lithium ion conductors, with a liquid-like ionic conductivity of about 12 mS/cm at room temperature. Unfortunately, LGPS also exhibits a very narrow (thermodynamic) electrochemical stability window of about 0.3 V (about 2.1 to about 2.4 V vs. Li/Li^+). Computational and experimental studies have reported that metallic and ionically insulating reaction products form on a lithium metal anode interface when operated outside of this electrochemical stability window. This constrains the effective operating range of LGPS to a small fraction of the about 4 V range specified in a typical Li-ion battery (about 3.8 V to about 0.1 V vs. Li/Li^+ for a transition metal oxide/graphite cell).

[0004] It is against this background that a need arose to develop embodiments of this disclosure.

Summary

[0005] All-solid-state Li-ion batteries (SSLIBs) hold promise as safer, longer lasting, and more energy dense alternatives to lithium-ion batteries (LIBs) with liquid electrolytes.

However, the identification and design of suitable solid electrolyte materials for use in SSLIBs has remained a significant engineering challenge. A high performance solid electrolyte should simultaneously exhibit fast Li ion conduction, negligible electronic conduction, and robust electrochemical stability. The material should also be formed from inexpensive and low mass elements in order to ensure cost competitiveness and high energy density. Ceramic materials are an attractive class of materials for this application, but other proposed ceramic lithium electrolyte materials falter on at least one of these desired properties. Some embodiments of this disclosure are directed to solid electrolytes from the lithium-boron-sulfur (LBS) chemical system, which display desired values for all these properties, comparable to or exceeding those of the best reported ceramic electrolyte materials.

[0006] Some embodiments of this disclosure are directed to a ceramic material with high performance as a solid-state electrolyte. It can find use in various devices that involve Li ion transport through a solid-state material. For example, the ceramic material can be used in a Li-ion battery as a solid-state electrolyte or as an electrode additive to improve Li ion conduction. As another example, the ceramic material can be used in electrochemical windows that involve lithium as an active species. In some embodiments, the ceramic material has an overall composition given by the stoichiometry $Li_aB_bS_c$, where b/c (or $1:x$) is, for example, in a range of about 7/13 (or about 1:1.9) to about 1/3 (or 1:3), and exhibits high Li ion conductivity and low electronic conductivity over the range of b/c values. In some embodiments, the ceramic material is composed of a mixture of fast ion conducting crystalline phases over the range of b/c values.

[0007] Advantageously, a ceramic material of some embodiments combines exceptional ionic conductivity and an exceptional electrochemical stability window. Additionally and unlike other materials that undergo unwanted reactions at a cathodic and/or an anodic interface, the ceramic material can achieve its high performance through a mechanism in which the material can undergo several reactions or phase changes while continuing to perform. In particular, the material produces favorable interfacial reaction products that are (1) electronically insulating and (2) ionically conducting when undergoing spontaneous, electrochemically-driven phase changes. The incorporation of dopants or additives can further improve performance of the material.

[0008] In some embodiments, a battery includes: (1) a cathode; (2) an anode; and (3) a solid-state electrolyte disposed between the cathode and the anode. At least one of the cathode, the anode, or the solid-state electrolyte includes a ceramic material including lithium

(Li), boron (B), and sulfur (S), the ceramic material includes multiple crystalline phases and has an overall composition given by *a*:*b*:*c* molar ratio of Li:B:S, and *c*/*b* is in a range of about 1 to about 3.

[0009] In some embodiments, a battery includes: (1) a cathode; (2) an anode; and (3) a solid-state electrolyte disposed between the cathode and the anode. At least one of the cathode, the anode, or the solid-state electrolyte includes a crystalline material including lithium (Li), boron (B), and sulfur (S), and a molar ratio of S:B is about 1 or greater.

[0010] In some embodiments, a battery includes: (1) a first electrode; (2) a second electrode; and (3) an electrolyte disposed between the first electrode and the second electrode. At least one of the first electrode or the second electrode includes an electrode additive including a lithium boron sulfide.

[0011] In some embodiments, a method includes: (1) providing a ceramic material including lithium (Li), boron (B), and sulfur (S), wherein the ceramic material includes multiple crystalline phases and has an overall composition given by *a*:*b*:*c* molar ratio of Li:B:S, and *c*/*b* is in a range of about 1 to about 3; and (2) applying an electrical potential across the ceramic material to transport lithium ions through the ceramic material.

[0012] Other aspects and embodiments of this disclosure are also contemplated. The foregoing summary and the following detailed description are not meant to restrict this disclosure to any particular embodiment but are merely meant to describe some embodiments of this disclosure.

Brief Description of the Drawings

[0013] For a better understanding of the nature and objects of some embodiments of this disclosure, reference should be made to the following detailed description taken in conjunction with the accompanying drawings.

[0014] Figure 1: Temperature dependence of Li ionic conductivity for $Li_5B_7S_{13}$, $Li_2B_2S_5$, and Li_3BS_3. Density functional theory molecular dynamics (DFT MD) simulation is performed at 900 K, 700 K, and 400 K for three materials from the LBS system, namely $Li_5B_7S_{13}$, $Li_2B_2S_5$, and Li_3BS_3. $Li_5B_7S_{13}$ was also simulated at 293 K. Computation is performed of an average Bader charge on Li and a slope of Li mean squared displacement (MSD) curves, then equations (3) and (4) in Example 1 are used to compute the Li ionic conductivity. These values represent an average of diagonal elements of a conductivity tensor. The diffusivity is determined from a slope of the MSD curve. The error bars represent the 75^{th} and 25^{th} percentile of slopes in the diffusivity considering all time origins from 0 to

75% of a final run time in 10 fs intervals. If Arrhenius dynamics are assumed, the high temperature ionic conductivity extrapolates to give the following RT ionic conductivities: 74 mS/cm, 10 mS/cm, and 2 mS/cm, respectively. This would make $Li_5B_7S_{13}$ over five times more conductive than LGPS and one of fastest solid Li ion conductors predicted to date.

[0015] Figure 2: Ternary phase diagram of the LBS system. $Li_5B_7S_{13}$, $Li_2B_2S_5$, and Li_3BS_3 are predicted to be Li superionic conductors at room temperature. This indicates that at least one of these three superionic phases may be present in various LBS compositions, indicating the LBS system may exhibit fast Li-ion conduction even when a material composition changes via interfacial degradation.

[0016] Figure 3: Analysis of electrochemical stability. According to grand potentials computed with Perdew-Burke-Ernzerhof density functional theory (PBE DFT), a mixture of LBS phases is thermodynamically stable from about 1.6 to about 2.2 V vs. Li/Li+. From about 1.0 to about 1.6 V and about 2.2 to about 3.8 V, the superionic LBS phases are predicted to become thermodynamically unstable but may remain kinetically stable. Below about 1.0 V and above about 3.8 V, the phases become further thermodynamically destabilized and are less likely to be kinetically stable. The effective energetics of the LBS mixture are denoted by the dotted black line; the mixture is predicted to be more electrochemically stable than any of the individual phases alone. The full reaction is provided at the bottom of the figure; formulas written in lighter shading correspond to fast ion conducting, non-electron conducting phases, and formulas written in dark shading correspond to non-ion conducting, non-electron conducting phases. The thermodynamically stable range of about 1.6 to about 2.2 V in the mixture is twice as wide as the predicted stability window of LGPS (about 2.1 to about 2.4 V). The error bars on the electrochemical window are associated with an uncertainty in the DFT energy calculations of 0.1 eV/atom.

[0017] Figure 4: Superionic molar fraction versus composition and potential. The molar fraction of thermodynamically stable superionic phases is plotted as a function of the B/(B+S) molar ratio and electrode potential. The optimal B/(B+S) ratios are those which exhibit a high molar fraction of superionic phases over the widest potential range. No superionic phases are predicted to be thermodynamically stable below about 1.6 V or above about 2.2 V vs. Li/Li^+, although high kinetic barriers may render them metastable (see Figure 3). The B/(B+S) ratios associated with pure phases are denoted with horizontal lines. The highest molar fraction of superionic phases over the widest potential range occurs with a B/(B+S) ratio of about 0.25 to about 0.35 (B:S molar ratio of about 1:1.9 to about 1:3). The

widest effective electrochemical stability window is predicted to be achieved with a B:S molar ratio of about 1:2.5.

[0018] Figure 5: Solid electrolyte performance characteristics. The plot provides thermodynamic electrochemical stability window widths computed with PBE DFT and experimentally reported ionic conductivities (on log-log scale) of several solid Li-ion conductors, including predicted values for a $Li_aB_bS_c$ ($2 \leq c/b \leq 2.5$) phase mixture electrolyte. The overall ionic conductivity of 36 mS/cm in LBS is computed by taking a weighted mean of bulk ionic conductivities of $Li_5B_7S_{13}$, $Li_2B_2S_5$ and Li_3BS_3, where weights are proportional to the thermodynamic electrochemical stability window widths of the phases. Taking the ionic conductivity as an indicator of power density and the electrochemical stability as an indicator of energy density, LBS is predicted to provide about twice the energy density of LGPS and about three times the power density. By comparison, LLZO exhibits a stability window five times wider than LBS, but an ionic conductivity value over 100 times lower.

[0019] Figure 6: Comparison of a X-ray diffraction (XRD) pattern of a resulting product (obtained from synthesis of Li_3BS_3) and a reference XRD pattern for Li_3BS_3.

[0020] Figure 7: Comparison of a XRD pattern of a resulting product (obtained from synthesis of $Li_2B_2S_5$) and a reference XRD pattern for $Li_2B_2S_5$.

[0021] Figure 8: Comparison of a XRD pattern of a resulting product (obtained from synthesis of $Li_5B_7S_{13}$) and a reference XRD pattern for $Li_5B_7S_{13}$.

[0022] Figure 9: Impedance spectra (Nyquist plots) of a synthesized Li_3BS_3 product, a synthesized $Li_2B_2S_5$ product, and a synthesized $Li_5B_7S_{13}$ product. Panel (a) provides a zoomed-in view about an origin, and panel (b) provides a full-range view.

[0023] Figure 10: Schematic of a battery according to some embodiments.

Description

[0024] Some embodiments are directed to a battery 100, which includes a cathode (or a first electrode) 102, an anode (or a second electrode) 106, and an electrolyte 104 disposed between and in contact with the cathode 102 and the anode 106 (see Figure 10). In some embodiments, the battery 100 is a lithium-ion (Li-ion) battery, the cathode 102 includes an active cathode material such as a transition metal oxide (e.g., lithium cobalt oxide ($LiCoO_2$), lithium manganese oxide ($LiMn_2O_4$), lithium nickel manganese cobalt oxide ($LiNi_xMn_yCo_zO_2$), or lithium iron phosphate ($LiFePO_4$)), and the anode 106 includes an active anode material such as graphite or another carbonaceous material.

[0025] In some embodiments, the electrolyte 104 is a solid-state electrolyte. In some embodiments, the electrolyte 104 includes a ceramic material including lithium (Li), boron (B), and sulfur (S). In some embodiments, the ceramic material is a crystalline material. In some embodiments, the ceramic material is a crystalline lithium boron sulfide or a crystalline lithium thioborate.

[0026] In some embodiments, the ceramic material has an overall composition given by the stoichiometry of *a*:*b*:*c* molar ratio of Li:B:S. In some embodiments, *a*/*b* is in a range of about 0.5 to about 3, about 0.5 to about 2.5, about 0.5 to about 2, about 0.5 to about 1.5, about 0.5 to about 1, about 0.7 to about 3, about 0.7 to about 2.5, about 0.7 to about 2, about 0.7 to about 1.5, or about 0.7 to about 1, and *c*/*b* is in a range of about 1 or greater, about 1 to about 9, about 1 to about 8, about 1 to about 7, about 1 to about 6, about 1 to about 5, about 1 to about 4, about 1 to about 3, about 13/7 to about 3, about 13/7 to about 2.5, about 2.5 to about 3, about 1.3 to about 2.7, about 1.5 to about 2.5, about 1.7 to about 2.3, about 13/7, about 2.5, or about 3. In some embodiments, *a*/*b* is less than about 1, and *c*/*b* is in a range of greater than about 13/7 and less than about 2.5. In some embodiments, *a*/*b* is greater than about 1, and *c*/*b* is in a range of greater than about 2.5 and less than about 3. In some embodiments, the ceramic material includes one or more crystalline lithium boron sulfide phases. In some embodiments, the ceramic material includes multiple lithium boron sulfide crystalline phases.

[0027] In some embodiments, the ceramic material includes at least one crystalline phase selected from $Li_5B_7S_{13}$, Li_3BS_3, and $Li_2B_2S_5$. In some embodiments, the ceramic material includes at least two different crystalline phases selected from $Li_5B_7S_{13}$, Li_3BS_3, and $Li_2B_2S_5$. In some embodiments, the ceramic material includes $Li_5B_7S_{13}$ and $Li_2B_2S_5$. In some embodiments, the ceramic material includes Li_3BS_3. In some embodiments, the ceramic material includes $Li_5B_7S_{13}$. In some embodiments, the ceramic material includes $Li_2B_2S_5$. In some embodiments, the ceramic material includes an additional phase including S or elemental sulfur.

[0028] In some embodiments, the ceramic material includes a first phase including $Li_5B_7S_{13}$ and a second phase including $Li_2B_2S_5$. In some embodiments, a molar ratio of the first phase to the second phase is in a range of about 0.1 to about 10, about 0.2 to about 5, about 0.3 to about 3, about 0.4 to about 2, about 0.5 to about 1.5, about 0.5 to about 1, about 0.6 to about 1.4, about 0.7 to about 1.3, about 0.8 to about 1.2, about 0.9 to about 1.1, about 0.5, or about 1. In some embodiments, the molar ratio of the first phase to the second phase is about 1, less than about 1, or greater than about 1. In some embodiments, the ceramic

material includes a third phase including Li_3BS_3, in addition to, or alternatively to, the first phase and the second phase.

[0029] In some embodiments, the ceramic material includes a first phase including $Li_2B_2S_5$ and a second phase including Li_3BS_3. In some embodiments, a molar ratio of the first phase to the second phase is in a range of about 0.1 to about 10, about 0.2 to about 5, about 0.3 to about 3, about 0.4 to about 2, about 0.5 to about 1.5, about 0.5 to about 1, about 0.6 to about 1.4, about 0.7 to about 1.3, about 0.8 to about 1.2, about 0.9 to about 1.1, about 0.5, or about 1. In some embodiments, the molar ratio of the first phase to the second phase is about 1, less than about 1, or greater than about 1. In some embodiments, the ceramic material includes a third phase including $Li_5B_7S_{13}$, in addition to, or alternatively to, the first phase and the second phase.

[0030] In some embodiments, the electrolyte 104 includes a first interfacial region adjacent to the cathode 102, and a second interfacial region adjacent to the anode 106. In some embodiments, the first interfacial region includes $Li_5B_7S_{13}$ and $Li_2B_2S_5$. In some embodiments, the first interfacial region also includes BS_2. In some embodiments, the second interfacial region includes $Li_5B_7S_{13}$ and $Li_2B_2S_5$. In some embodiments, the second interfacial region also includes Li_3BS_3. In some embodiments, the second interfacial region also includes Li_2S. In some embodiments, the second interfacial region also includes B or elemental boron.

[0031] In additional embodiments, the ceramic material according to any of the foregoing embodiments is incorporated as an electrode additive in either, or both, of the cathode 102 and the anode 106. For example, the ceramic material can be incorporated in the form of particles dispersed along with an active cathode material or an active anode material. In additional embodiments, the ceramic material according to any of the foregoing embodiments is incorporated as a coating in either, or both, of the cathode 102 and the anode 106. For example, the ceramic material can be incorporated as a coating over an active cathode material or an active anode material.

[0032] Additional embodiments are directed to a method, which includes providing the cathode 102, providing the anode 106, and providing the electrolyte 104 disposed between and in contact with the cathode 102 and the anode 106. In some embodiments, the method includes providing the ceramic material according to any of the foregoing embodiments, and applying an electrical potential across the ceramic material, via the cathode 102 and the anode 106, to transport lithium ions through the ceramic material.

Examples

[0033] The following examples describe specific aspects of some embodiments of this disclosure to illustrate and provide a description for those of ordinary skill in the art. The examples should not be construed as limiting this disclosure, as the examples merely provide specific methodology useful in understanding and practicing some embodiments of this disclosure.

Example 1

Solid Li-ion electrolyte from crystalline lithium-boron-sulfur chemical system

[0034] Overview

[0035] This example reports a solid-state Li-ion electrolyte predicted to exhibit simultaneously fast ionic conductivity, wide electrochemical stability, low cost, and low mass density. Three phases are identified within the crystalline lithium-boron-sulfur (LBS) system, $Li_5B_7S_{13}$, $Li_2B_2S_5$ and Li_3BS_3, with exceptional density function theory (DFT) based single crystal ionic conductivity values at room temperature of about 74 mS/cm, about 10 mS/cm, and about 2 mS/cm, respectively. Computation is performed of the thermodynamic electrochemical stability window widths of these materials to be about 0.50 V, about 0.16 V, and about 0.45 V. Individually, these materials exhibit similar or improved ionic conductivity and electrochemical stability to the best available sulfide-based solid-state Li-ion electrolyte materials, including $Li_{10}GeP_2S_{12}$. However, it is predicted that electrolytes synthesized from a range of compositions in LBS system can exhibit even wider thermodynamic electrochemical stability windows of about 0.6 V and potentially as high as about 3 V or greater. It is predicted that a range of boron-to-sulfur molar ratios for achieving high ionic conductivity over an electrochemical stability window wider than about 0.5 V range to be about 1:2 to about 1:2.5. LBS phase mixtures within this range of compositions also have low elemental cost of about 0.05 USD/m^2 per 10 μm thickness, significantly lower than that of germanium-containing LGPS, and a comparable mass density below 2 g/cubic centimeter (cc).

[0036] Introduction

[0037] Ionic conductivity and electrochemical stability can be inversely correlated, indicating that optimal materials are outliers and likely to be very difficult to identify. An alternative approach is proposed to the strategy of searching for one material that simultaneously optimizes both criteria: identifying a high ionic conductivity solid material that breaks down into fast ion conducting and electronically insulating phases at both EEIs. In

this scenario, a wider electrochemical window can be achieved because the electrolyte passes through more phase transitions before poor ion conductors actually appear.

[0038] It is predicted that crystalline LBS is a material system that can demonstrate this capability: a phase mixture of fast ion conducting phases from the LBS system, $Li_5B_7S_{13}$, $Li_2B_2S_5$, Li_3BS_3, over a range of boron-to-sulfur ratios will oxidize and reduce into ionically conducting and electronically insulating interfacial products, providing electrochemical stability over a wider potential range than any of the individual phases alone.

[0039] Lithium ion conducting glasses from the B_2S_3-Li_2S system can have a room temperature lithium ion conductivity of about 10^{-4} S/cm. Doping with LiI can increase the lithium conductivity by an order of magnitude, but the oxidation of iodine results in too narrow of an electrochemical stability window for use in SSLIBs. Here, in this example, DFT calculations on single crystals indicate that several phases in the crystalline LBS system can have even higher room temperature ionic conductivity (about 10^{-2} S/cm) without the addition of iodine, and a wide electrochemical stability window can be realizable. Sulfide-based glassy conductors tend to be quite hygroscopic as well and crystalline materials can provide improved moisture and thermal stability. The properties of the LBS system are explained below.

[0040] Ionic conductivity

[0041] Evaluation is performed of the ionic conductivity of several phases in the LBS system. Three thermodynamically stable phases exist that exhibit liquid-like lithium ion conduction at room temperature: $Li_5B_7S_{13}$, Li_3BS_3 and $Li_2B_2S_5$. These three crystalline phases have space groups Cc, Pnma, and Cmcm, respectively.

[0042] To predict the room temperature (RT) ionic conductivity in $Li_5B_7S_{13}$, $Li_2B_2S_5$, and Li_3BS_3, simulation of density functional theory molecular dynamics (DFT-MD) is performed on single crystals of these materials at 900 K, 700 K, and 400 K, leveraging the Perdew-Burke-Ernzerhof (PBE) methodology of the generalized gradient approximation and the projector augmented wave (PAW) method. Diffusion in $Li_5B_7S_{13}$ at 293 K was fast enough that it could observed during simulation: 0.013 (+0.006, -0.012) $Å^2$/ps. Ionic diffusion in solids is generally not isotropic; this three-dimensional diffusivity value corresponds to a mean of diagonal elements of a diffusion tensor, or one-third of a trace. The Methods section provides further simulation details.

[0043] In Figure 1, the logarithm of ionic conductivity is plotted versus inverse temperature, and fast Li conduction in all three materials is confirmed at RT when Arrhenius dynamics are assumed. The RT Li conductivity of $Li_5B_7S_{13}$ in particular is remarkable: 74

(+31, -68) mS/cm when simulated at RT and 62 (+9, -2) mS/cm when extrapolated from high temperature. This is several times higher than that of LGPS (about 12 mS/cm). The other two materials have exceptional predicted RT ionic conductivities as well when extrapolated from high temperature: 10 (-5, -10) mS/cm for $Li_2B_2S_5$ and 2 (+1, -2) mS/cm for Li_3BS_3. To compute uncertainties in these values, extrapolation is performed down to RT along upper and lower limits of the high temperature uncertainties. The Methods section provides further discussion of calculating the uncertainties. These predictions for single crystals place the LBS materials among the best reported Li-ion conductors.

[0044] Band gaps of $Li_5B_7S_{13}$, $Li_2B_2S_5$, and Li_3BS_3 are computed with PBE DFT to be 3.6, 2.4, and 3.1 eV, respectively. A high band gap in solid electrolyte materials is desired in order to reduce electrical conductivity and enhance electrochemical stability. Although the electrical conductivity depends on both the electronic density of states and the band gap, calculations for pure Si demonstrate that a true band gap of 1 eV or higher leads to acceptably small levels of electron conduction. Assuming a minimum acceptable band gap of 1 eV, the calculations predict that the band gaps are sufficiently large for the LBS phases to be desirable in solid electrolyte applications. Furthermore, the band gap (in eV) is an upper bound on the thermodynamic electrochemical stability window width (in V) so larger band gaps can indicate more robust electrochemical stability. PBE DFT simulations tend to underestimate the true band gap by a factor of two or more, so the true band gaps may be higher than the values reported here. These calculations leverage the Automatic-FLOW (AFLOW) for Materials Discovery *k*-point path generator and the P4VASP visualization tool.

[0045] Reactions at an electrode-electrolyte interface

[0046] A ternary LBS phase diagram as generated by the Materials Project is provided in Figure 2. It is noted the three fast conducting phases identified here are the predicted stable phases on the interior of the phase diagram.

[0047] Giving that there are three excellent lithium ion conductors in the LBS chemical space, the next stage is to identify an optimal composition and an operating range for use as an electrolyte. This involves predicting phases that will form when the electrolyte is oxidized/reduced by a cathode and an anode at an EEI. Examination is first performed for thermodynamics, and then examination returns to kinetics in the following section.

[0048] The thermodynamic approach to predicting electrochemical stability entails evaluating a grand potential function Φ for all phases at a given applied Li chemical potential μ_{Li} and computing the convex hull. Phases on the convex hull of the grand potential function are electrochemically stable against the applied potential. Since electrodes operate by

inserting or removing Li from an electrolyte, applying an electrode at a given potential (in V vs. Li/Li^+) corresponds to applying a lithium chemical potential of opposite sign (in eV/atom). The grand potential function is computed as:

$$\Phi = E - \mu_{Li} N_{Li} \quad (1)$$

where E is the standard formation enthalpy of the phase per formula unit, μ_{Li} is the (negative) applied chemical potential in eV, N_{Li} is the number of Li atoms in the phase per formula unit, and $\Sigma_{i \neq Li} N_i$ is the number of non-Li atoms per formula unit. For simplicity, it is assumed the entropic contribution to enthalpy is negligible and the enthalpy is replaced with the DFT-computed standard formation energy.

[0049] The grand potential function is computed for all stable crystalline phases of the LBS system in the Materials Project over a range of applied potentials from 0 to 5 V vs. Li/Li^+. At each applied potential, computation is performed of the energy above the convex hull of all relevant phases. The energies above the hull versus applied potential are given in Figure 3. The predicted electrochemical stability window of a material is given by the range of potentials (horizontal axis values in Figure 3) for which the material has zero energy above the hull (vertical axis values in Figure 3). Figure 3 indicates that the three fast conducting phases have the following electrochemical stability windows: 0.16 V for $Li_2B_2S_5$, 0.45 V for Li_3BS_3, and 0.50 V for $Li_5B_7S_{13}$. The Methods section provides computational details on the construction of the convex hull.

[0050] To achieve enhanced electrochemical stability, examination is made of the performance of phase mixtures of these fast conducting structures over a range of boron-to-sulfur ratios. In such a mixture, the electrolyte can transform into ion conducting products that permit function over a wider electrochemical range than the individual phases alone. The predicted interfacial chemistry of this composition is set forth below.

[0051] Electrochemical stability of LBS mixture

[0052] It is predicted that more favorable EEI products and therefore function over a wider electrochemical stability can be achieved with a mixture of fast conducting LBS phases. In a closed system, the Gibbs phase rule predicts up to three phases can coexist in a ternary chemical space; but when a Li chemical potential is introduced this decreases to two. The 1 to 2 phases predicted to be thermodynamically stable at a given potential and their molar fractions depend on a molar ratio of boron-to-sulfur in a composition. Figure 4 provides a molar fraction of thermodynamically stable superionic phases as a function of potential and

boron-to-sulfur molar ratio. Desired compositions are those which yield the widest electrochemical window with the largest molar fraction of superionic phases. It is predicted that a desired composition includes a B molar ratio (relative to a combined molar amount of B and S) of about 0.29 to about 0.33, or a B:S molar ratio of about 1:2 to about 1:2.5. One example starting composition would be a mixture $Li_5B_7S_{13}$ + $2Li_2B_2S_5$ (B:S = 1:2.09). The LBS phase diagram predicts this composition will remain a phase separated mixture. This specific mixture (B:S = 2.09) is referred to as a "starting structure" for the remainder of this example, but this analysis can apply to any other combination of two of the three fast conducting phases within the about 1:2 to about 2.5 B:S ratio. Consideration is made of both thermodynamic and kinetic factors that could influence the electrochemical stability of such a phase mixture.

[0053] According to calculations, the two phases in the starting structure ($Li_5B_7S_{13}$ and $Li_2B_2S_5$) sit on the convex hull (and therefore are thermodynamically stable) from about 2.0 to about 2.1 vs. Li/Li^+. As the voltage increases beyond about 2.1 V, the dissolution of $Li_5B_7S_{13}$ and formation of BS_2 are thermodynamically favored; the stable interfacial products are predicted to be $Li_2B_2S_5$ and BS_2. The decomposition of $Li_2B_2S_5$ becomes favored at about 2.2 V. Above this range, the thermodynamically stable products are predicted to be LiS_4 and BS_2. Excess lithium will be taken up by the cathode. It is noted that BS_2 is a non-electron conducting material as inferred from its large bandgap of about 2.6 eV as calculated by PBE DFT. After a phase transition to BS_2 occurs, it is likely that regions of BS_2 with some intercalated Li will be present, as different phases within solid materials often have some regions of overlap. These regions may be good Li-ion conductors that would allow the continued flow of ionic current through the electrolyte to the cathode (and, therefore, operation past the 2.2 V threshold). To understand the ion conduction characteristics of slightly lithiated BS_2, DFT-MD of $Li_{0.03}BS_2$ and $Li_{0.09}BS_2$ is performed at 900 K. Observation is made of diffusivities on the order of 1 $Å^2$/ps over about 10 ps of simulation, indicating Li intercalants in BS_2 may conduct as well as the Li in $Li_5B_7S_{13}$, $Li_2B_2S_5$, and Li_3BS_3.

[0054] The thermodynamically stable phase of LiS_4 is a molecular solid and is likely to be non-electron conducting due to its large PBE DFT-calculated bandgap of about 2.2 eV, greater than the minimum threshold of 1 eV. It is assumed that LiS_4 is a poor Li conductor, even with small amounts of intercalated Li, because of the molecular structure with large amounts of vacuum space between molecules that Li ions are unlikely to traverse.

[0055] As the potential increases further, the energy above the hull of $Li_5B_7S_{13}$ and $Li_2B_2S_5$ is predicted to rise linearly; the energy difference is about 0.2 eV/atom for both structures at 3

V, and it is about 0.4 eV/atom at 3.8 V. In this regime of thermodynamic instability, kinetic considerations come into play. A significant energy difference is likely to be involved to drive the rearrangement of atoms to form LiS_4 and BS_2. The formation of these off-stoichiometry phases will involve long-range diffusion of B and S, which is likely to have a significant associated energy barrier. In fact, the DFT-MD simulations of all three superionic LBS phases show no migration of B or S over the hundreds of picoseconds timescale at 900 K, in contrast to the significant Li migration that is observed. Some B or S diffusion would be observed in these simulations if the energy barrier to long-range B or S diffusion was small enough for such diffusion to be facile. The absence of any B or S diffusion on these simulation timescales indicates that the diffusion barrier for B and S is significant, likely larger than 0.4 eV, an approximate upper bound ion conduction energy barrier in reasonably conductive materials. Thus it is possible the fast ion conducting phases in the starting structure will remain kinetically stabilized in this range or beyond. Eventually, as the potential increases, the energy difference will become large enough to drive the diffusion to form the degradation products LiS_4 and BS_2; this potential specifies the upper threshold of anodic stability of the LBS phase mixture. If it is assumed the energy above the hull for rearrangement is 0.4 eV/atom, the anodic stability threshold on the cathode side with kinetic stabilization is about 3.8 V.

[0056] On the anode side (cathodic stability), $Li_2B_2S_5$ is predicted to become thermodynamically unfavorable at voltages below about 2.0 V. In this regime $Li_2B_2S_5$ is replaced by superionic Li_3BS_3 on the convex hull, so Li_3BS_3 is predicted to form in its place. This is a fortunate result, as the formation of the poor ion conductor Li_2S would be thermodynamically favored if the fast-conducting Li_3BS_3 was not present in the LBS phase diagram. In the about 1.6 to about 2.0 V range, Li_3BS_3 and $Li_5B_7S_{13}$ are predicted to be thermodynamically stable.

[0057] Kinetic considerations are again likely to be important in this phase change; the predicted energy above the hull for $Li_2B_2S_5$ is no larger than 0.1 eV/atom in the 1.6-2.0 V range, so $Li_2B_2S_5$ may remain kinetically stabilized. However, the possible decomposition of $Li_2B_2S_5$ is acceptable because the resulting degradation product is Li_3BS_3.

[0058] Below about 1.6 V, both Li_3BS_3 and $Li_5B_7S_{13}$ lift off the convex hull. Their energy above the hull increases to 0.2 eV/atom at about 1.4 V for $Li_5B_7S_{13}$ and about 1.3 V for Li_3BS_3, and approaches 0.4 eV/atom at about 1.2 V for $Li_5B_7S_{13}$ and about 1.0 V for Li_3BS_3. The resulting thermodynamically favored products, if kinetically accessible, are Li_2S and elemental B. Li_2S is an electron insulator that is reported to exhibit poor (but non-zero)

lithium ion conduction (about 10^{-13} S/cm), while elemental B in its ground state is also an electron insulator and is unlikely to conduct lithium. The formation of Li_2S and elemental B will again involve significant long-range diffusion, and the barrier to this diffusion could feasibly kinetically stabilize the electrolyte against such a degradation. If this degradation does occur, all fast ion conductors will give rise to slow ion conductors and battery operation will cease.

[0059] A question for the cathodic stability of the LBS system is which phase of elemental boron will form. The PBE DFT calculations in the Materials Project database predict the ground state of boron to be a semiconductor with predicted band gap of about 1.4 eV, but DFT also predicts metallic phases to be kinetically accessible by as little as about 0.1 eV/atom. It is also possible that metallic Li-B alloys will form on the anode. If metallic phases form, the electron insulating criteria outlined above will not be satisfied, and interfacial products will not passivate a surface from further reaction.

[0060] At much lower potentials (0 to about 0.3 V) the driving force for degradation becomes much larger (> 1 eV/atom for Li_3BS_3 and $Li_5B_7S_{13}$) and the thermodynamically favored products are Li_2S and metallic LiB. The original phases are unlikely to persist in this regime, but the LBS material may be suitable for use in solid-state batteries with Li metal anodes if these phases can be kinetically stabilized at these low potentials.

[0061] This predicted electrochemical stability behavior is summed up by the regions of thermodynamic stability, possible kinetic stability, and unlikely kinetic stability noted in Figure 3. By using an LBS mixed phase within the about 1:2 to about 1:2.5 B:S ratio, the stability characteristics of the individual phases are combined: the mixture combines the stronger cathodic stability of Li_3BS_3, the stronger anodic stability of $Li_2B_2S_5$, the fast conductivity of $Li_5B_7S_{13}$, and has a thermodynamic stability window (about 0.6 V) wider than any of the individual phases alone (about 0.16 V, about 0.45 V, and about 0.5 V). The effective energy above the hull of the LBS phase mixture is denoted with a dotted black line on Figure 3. This effective energy above the hull of the phase mixture follows the envelope of the three LBS phases. The overall reaction for a boron-to-sulfur ratio of 1:x ($2 \leq x \leq 2.5$), with associated thermodynamic potentials, is:

$$xLi_2S + B \xleftrightarrow{1.37} (0.88x - 1.63)Li_3BS_3 + (0.38 - 0.13x)Li_5B_7S_{13} \xleftrightarrow{2.03} (0.78x - 1.44)Li_2B_2S_5 + (0.56 - 0.22x)Li_5B_7S_{13} \xleftrightarrow{2.07} (x - 2.0)Li_2B_2S_5 + (2.0 - 2.0x)BS_2 \xleftrightarrow{2.19} (0.25x - 0.5)LiS_4 + BS_2$$

(2A)

[0062] Provided the anode potential is above about 0.36 V, Li_2S and B are likely to form on the anode interface; LiS_4 and BS_2 are likely to form on the cathode if the potential is above about 2.19 V. This operating regime may be well-suited to solid-state battery applications where a smaller voltage is acceptable, such as batteries in internet of things (IoT) devices. Nonetheless, it is feasible that kinetic stabilization will allow these materials to operate beyond this potential window and potentially up to > about 4 V without degrading. An additional strategy for realizing a wider potential window if desired might be to combine this electrolyte with degradation resistant materials in a two- or three-electrolyte architecture.

[0063] Mixtures with different B:S ratios exhibit different predicted reaction trajectories which may be suboptimal in comparison to the trajectory in Eq. (2A). For B:S ratios of 1:x ($x \geq 3$), the overall reaction is:

$$xLi_2S + B \xleftrightarrow{1.89} Li_3BS_3 + (x-3)Li_2S \xleftrightarrow{2.04} Li_3B_2S_5 + (x-2.5)Li_2S \xleftrightarrow{2.14} 0.5Li_2B_2S_5 + (0.25x - 0.63)LiS_4 \xleftrightarrow{2.19} (0.25x-0.5)LiS_4 + BS_2$$

(2B)

This regime is suboptimal because a non-conductor is always present: Li_2S, B, or LiS_4.

[0064] For B:S ratios of 1:x ($2.5 < x < 3$), the overall reaction is:

$$xLi_2S + B \xleftrightarrow{1.89} 0.33xLi_3BS_3 + (1-0.33x)B \xleftrightarrow{1.63} (0.88x-1.63)Li_3BS_3 + (0.38 - 0.13x)Li_6B_7S_{13} \xleftrightarrow{2.02} (2x-5)Li_3BS_3 + (3-x)Li_2B_2S_5 \xleftrightarrow{2.04} Li_3B_2S_5 + (x-2.5)Li_2S \xleftrightarrow{2.14} 0.5Li_2B_2S_5 + (0.25x-0.63)LiS_4 \xleftrightarrow{2.19} (0.25x-0.5)LiS_4 + BS_2$$

(2C)

This reaction exhibits the same electrochemical stability window as the $2 \leq x \leq 2.5$ composition but is suboptimal for possessing lower molar fractions of superionic phases.

[0065] For B:S ratios of 1:x ($1.9 \leq x < 2$), the overall reaction is:

$$xLi_2S + B \xleftrightarrow{1.89} (0.88x-1.63)Li_3BS_3 + (0.38-0.13x)Li_6B_7S_{13} \xleftrightarrow{2.02} (0.76x-1.44)Li_2B_2S_5 + (0.56-0.22x)Li_6B_7S_{13} \xleftrightarrow{2.07} Li_6B_7S_{13} + (5.0-2.0x)BS_2 \xleftrightarrow{2.12} (2-x)B_2S_3 + (2x-3)BS_2$$

(2D)

which exhibits a slightly lower anodic stability threshold than the starting structure (about 2.12 V vs. about 2.19 V).

[0066] For B:S ratios of 1:x ($1.5 \leq x < 1.9$), the overall reaction is:

$$xLi_2S + B \xleftarrow{1.89} 0.33xLi_3BS_3 + (1 - 0.33x)B \xleftarrow{1.68} 0.077xLi_5B_7S_{13} + (1 - 0.54x)B \xleftarrow{1.67} (0.4x - 0.6)Li_5B_7S_{13} + (2.6 - 1.4x)B_2S_5 \xleftarrow{2.12} (2 - x)B_2S_5 + (2x - 3)BS_2 \quad (2E)$$

which exhibits a lower anodic stability threshold still.

[0067] The lowest anodic stability threshold occurs for B:S ratios of 1:x ($0 \leq x < 1.5$), where the reaction is:

$$xLi_2S + B \xleftarrow{1.89} 0.33xLi_3BS_3 + (1 - 0.33x)B \xleftarrow{1.68} 0.077xLi_5B_7S_{13} + (1 - 0.54x)B \xleftarrow{1.67} 0.33xB_2S_5 + (1 - 0.67x)B \quad (2F)$$

[0068] The expected error in the electrochemical window of Figure 3 is calculated numerically by assuming an uncertainty of ± 100 meV/atom in the DFT energy calculations and propagating this error through the calculation of the convex hull. The energies of all phases are altered by an amount dE chosen uniformly at random on the interval [-100 meV/atom, +100 meV/atom], the convex hulls at all potentials from 0-5 V vs. Li/Li^+ are constructed, and the three regions of electrochemical stability from Figure 3 are computed. This process is repeated continuously until the standard deviation of the end points of these regions is converged to within 1%. The error bars are shown on Figure 3. In about 8% of realizations, there is no region of thermodynamic stability, namely all fast conducting phases are above the convex hull. The error bars are about 0.3 V in width, indicating an uncertainty of ± 100 meV/atom results in relatively small uncertainties in the predicted electrochemical stability behavior.

[0069] Energy density and cost

[0070] Energy density and cost are important practical considerations for a battery material and should be incorporated into the materials discovery process. This is especially true for candidate SSLIB chemistries, since there should be potential for significant improvement over incumbent liquid electrolytes to become commercially attractive. In order to improve gravimetric energy density, solid electrolyte materials should be made of low mass elements. In this respect, lithium, boron, and sulfur are favorable elements. The densities of Li_3BS_3, $Li_5B_7S_{13}$, and $Li_2B_2S_5$ are about 1.65, about 2.06, and about 1.77 g/cc, respectively. This is a factor of about two less dense than LLTO ($Li_{0.5}La_{0.5}TiO_3$, about 4.68 g/cc) and LLZO ($Li_7La_3Zr_2O_{12}$, about 4.99 g/cc), and similar to that of LGPS (about 1.98 g/cc).

[0071] Current raw materials costs of Li, B, and S are about $20/kg, about $5/kg, and about $1/kg. At this price point, the raw materials cost of an LBS solid electrolyte will be in the

range about 0.05 USD per m^2 per 10 μm of thickness. Additionally, LBS omits germanium (about $500/kg), making the raw materials significantly cheaper than those in LGPS. Manufacturing will involve additional costs, and the magnitude of these costs will vary depending on the economics and scalability of the synthesis routes. Regardless, the cost of the raw materials indicates that LBS is a strong candidate for commercial manufacture at a cost below McCloskey's threshold of 10 USD per m^2 for lithium ion electrolytes. This cost target has since been adopted by the US Department of Energy's Advanced Research Projects Agency – Energy (ARPA-E).

[0072] Conclusions

[0073] The identification of solid lithium ion conductors that oxidize and reduce into non-metallic, ion conducting products at electrolyte-electrode interfaces would be a significant advancement towards realizing an all-solid-state lithium-ion battery with superior energy density to traditional lithium-ion batteries. To this end, computational investigation is performed of the electrolyte performance of a LBS phase mixture with $1{:}x$ ($2 < x \leq 2.5$) ratio of boron to sulfur. This material is predicted to exhibit liquid-like ionic conductivity (about 10^{-1}–10^{-3} S/cm) at room temperature and over a range of applied Li potentials. Thermodynamic and kinetic considerations indicate that fast lithium ion conductors may form or persist on electrode-electrolyte interfaces during electrolytic oxidation and reduction by electrodes. The LBS phase mixture is predicted to be effectively thermodynamically stable in a window of about 1.6 to about 2.2 V vs. Li/Li^+, similar to that of LGPS, and may be kinetically stabilized over an about 1.0 to about 3.8 V range and beyond. In Figure 5, a plot is shown of the performance characteristics of other Li-ion conductors and the characteristics of LBS predicted here. Taking ionic conductivity as indicative of power density and electrochemical stability window as indicative of energy density, this plot shows that LBS may offer a doubling of energy density over LGPS without significant loss in energy density.

[0074] This example sets forth an approach to enhancing electrochemical stability by combining fast ion conducting phases from a same chemical family. This approach could be extended to other solid electrolyte systems where multiple fast ion conducting phases exist and electrochemical stability is a concern. This example indicates that solid LBS electrolytes may offer comparable or significantly improved performance over other solid electrolytes in terms of ionic conductivity, electrochemical stability, materials cost, and weight.

[0075] Methods

[0076] *DFT molecular dynamics simulation*

[0077] For the simulation of DFT-MD in $Li_5B_7S_{13}$, $Li_2B_2S_5$, and Li_3BS_3, utilization is made of the Vienna Ab Initio Simulation Package (VASP) with the generalized gradient approximation (GGA) of Perdew-Burke-Ernzerhof (PBE) and the projector augmented wave (PAW) method. The unit cells are obtained from the Materials Project database. Simulation is performed of supercells of 99, 71, and 111 atoms, respectively, for about 10-100 ps at each temperature. One lithium vacancy is introduced per unit cell. The Li_sv, B, and S pseudopotentials are used, with a plane wave cutoff energy of 499 eV for all structures, and a gamma-point only *k*-mesh. This corresponds to a reciprocal lattice *k*-point density of 0.59, 0.68, and 0.48 nm^{-3}. The VASP input files are generated using the *pymatgen.io.vasp.sets* module of Pymatgen.

[0078] For the simulations of $Li_{0.03}BS_2$ and $Li_{0.09}BS_2$, one and three Li atoms are added, respectively, to a 96-atom supercell of BS_2. A gamma-point only *k*-mesh is used for a reciprocal lattice *k*-point density of 0.39 nm^{-3}.

[0079] *Ionic conductivity calculation*

[0080] To compute ionic conductivity from DFT-MD, the three-dimensional lithium diffusivity is first computed as a function of temperature $D(T)$, namely the average of the diagonal entries of the diffusivity tensor, and then the ionic conductivity is computed through the Einstein relation. $D(T)$ is computed from one-sixth of the slope of the mean squared displacement (MSD), $(\Delta r)^2$, of Li over time at a given simulation temperature:

$$D(T) = \frac{1}{6}\frac{(\Delta r)^2}{\Delta t} \tag{3}$$

[0081] There are thermal fluctuations in the MSD curves, which may be exacerbated by the shorter simulation times employed here. The slope of the MSD curve is taken as the median slope when considering all time origins up to 75% of the total simulation time, in 10 fs intervals. The uncertainty of the diffusivities is computed as the 25th and 75th percentiles of these distributions of slope values.

[0082] The diffusivities and uncertainties are calculated at 900 K, 700 K, and 400 K. Arrhenius dynamics is assumed to extrapolate the diffusivities to 293 K. In the case of $Li_5B_7S_{13}$, the RT diffusivity is computed directly from simulation, and close agreement is found with the Arrhenius extrapolation.

[0083] The RT diffusivities are converted to ionic conductivities using the Einstein relation:

$$\sigma(T) = \frac{D(T)nq^2}{k_B T} \tag{4}$$

where n is the Li ion number density and q is the average effective charge on Li ions. The average charge on Li is computed using the converged electron densities computed from DFT and the Bader charge analysis methods of Henkelman et al. In these DFT calculations a plane wave cutoff of 520 eV and a Monkhorst Pack k-point mesh with a density of at least 1000/atom are used. The Bader charge on $Li_5B_7S_{13}$, $Li_2B_2S_5$, and Li_3BS_3 is computed to be about 0.89, about 0.90, and about 0.88, respectively.

[0084] To compute the uncertainties associated with the extrapolation of conductivity to RT, a linear model is used along the upper and lower thresholds of the error bars (on log scale) versus inverse temperature for each composition. The predicted error bar width at inverse room temperature is assumed to be the difference in these two linear extrapolations at room temperature.

[0085] To confirm convergence in Li ionic conductivity with respect to unit cell size and Li vacancy concentration, DFT-MD simulation is performed in all three phases at 900K with doubled unit cells and zero Li vacancy concentration. For $Li_5B_7S_{13}$ and Li_3BS_3, very close alignment is found between the Li diffusivity of these simulations with the original simulations: about 0.88 vs. about 1.0 $Å^2$/ps for $Li_5B_7S_{13}$ and about 0.55 vs. about 0.61 $Å^2$/ps for Li_3BS_3. For $Li_2B_2S_5$, the doubled unit cell with zero Li vacancy concentration showed no Li diffusivity after 33 ps of simulation.

[0086] *Convex hull calculation*

[0087] To calculate the electrochemical stability windows provided in Figures 3 and 4, the grand potential $\Phi(\mu_{Li})$ of all phases is computed at a range of applied Li chemical potentials of $0 \leq \mu_{Li} \leq 5$ V vs. Li/Li^+ and the convex hull is constructed. The convex hull represents the lowest grand potential that can be accessed at a given composition and this specifies the thermodynamically stable phase(s).

[0088] For a grand potential phase diagram at a given chemical potential, a modified Graham scan methodology is used for drawing the convex hull. Beginning with the lowest grand potential end member on the left-hand side of the diagram, phase i, the angle θ_{ij} is computed from the horizontal formed when drawing a line from this phase to all other phases j. Setting θ_{ij} as zero along the positive y-axis and increasing counterclockwise, a search is made for the phase j^* that forms an angle closest to π provided that $\pi < \theta_{ij} < 2\pi$ (namely, j^* is down and to the right). This phase j^* is identified as sitting on the convex hull and a line is drawn between the two phases. For any phases k existing above the convex hull between phases i and j^*, the energy above the hull is computed as the grand potential difference between this line and the grand potential of phase k. The same procedure is then repeated,

with the search now spreading out from the new phase *j**. This is repeated until the search identifies the lowest potential end member on the right-hand side of the phase diagram.

Example 2

Synthesis and characterization of Li_3BS_3, $Li_2B_2S_5$, and $Li_5B_7S_{13}$

[0089] Synthesis of Li_3BS_3 and $Li_2B_2S_5$

[0090] Inside an argon-atmosphere glove box, stoichiometric amounts of Li_2S, elemental boron (amorphous), and elemental sulfur were mixed thoroughly with mortar and pestle until homogenous in color to the eye. This precursor mixture was then loaded into a carbon-coated quartz ampule, evacuated by roughing vacuum pump, and sealed by flame.

[0091] The sealed carbon-coated quartz ampule was then loaded into a custom-built furnace rig for melting. This furnace rig allowed for the rotation of the ampule during melting which aids in obtaining a substantially complete reaction in a single stage.

[0092] The ampule was heated at a rate of about 1°/min to about 750°C, held for about 2 hr at this temperature, and cooled to room temperature at about 5°/min.

[0093] After collecting and grinding each resulting material to powder, substantially pure-phase products are obtained.

[0094] Synthesis of $Li_5B_7S_{13}$

[0095] Synthesis procedures, temperatures, and times are similar to those for Li_3BS_3 and $Li_2B_2S_5$ described above. However, an extra heat treatment is applied to drive transition to the desired phase.

[0096] After synthesis, a resulting material is collected from a carbon-coated quartz ampule, reground thoroughly, and loaded into a fresh tube for heat treatment. A non-rotating furnace was used to ramp at about 5°/min to about 600°C, held for about 2 hr at this temperature, and ramp at about 5°/min to room temperature.

[0097] After collecting the material, nearly pure-phase products are obtained, with a small amount of original, pre-heat treatment phase remaining.

[0098] Characterization of Li_3BS_3, $Li_2B_2S_5$, and $Li_5B_7S_{13}$

[0099] Resulting products from synthesis were characterized by X-ray diffraction (XRD). Figure 5 compares a XRD pattern of a resulting product (obtained from synthesis of Li_3BS_3) and a reference XRD pattern for Li_3BS_3. As can be seen, there is good agreement in peak positions of the XRD pattern of the synthesized Li_3BS_3 product with respect to the reference XRD pattern, and no additional phase is detected, indicating that the synthesized Li_3BS_3

product is substantially pure-phase. Figure 6 compares a XRD pattern of a resulting product (obtained from synthesis of $Li_2B_2S_5$) and a reference XRD pattern for $Li_2B_2S_5$. As can be seen, there is good agreement in peak positions of the XRD pattern of the synthesized $Li_2B_2S_5$ product with respect to the reference XRD pattern, and no additional phase is detected, indicating that the synthesized $Li_2B_2S_5$ product is substantially pure-phase. Figure 7 compares a XRD pattern of a resulting product (obtained from synthesis of $Li_5B_7S_{13}$) and a reference XRD pattern for $Li_5B_7S_{13}$. As can be seen, there is good agreement in peak positions of the XRD pattern of the synthesized $Li_5B_7S_{13}$ product with respect to the reference XRD pattern. A small amount of an additional phase is detected (corresponding to $Li_{10}B_{10}S_{20}$).

[00100] The resulting products from synthesis were characterized by electrochemical impedance spectroscopy. Figure 8 shows impedance spectra (Nyquist plots) of the synthesized Li_3BS_3 product, the synthesized $Li_2B_2S_5$ product, and the synthesized $Li_5B_7S_{13}$ product. Ionic conductivities of the synthesized products were computed from the impedance spectra, as set forth in Table 1.

Material	Conductivity (S/cm)
Li_3BS_3	1.19×10^{-7}
$Li_2B_2S_5$	3.40×10^{-7}
$Li_5B_7S_{13}$	1.00×10^{-3}

[00101] As used herein, the singular terms “a,” “an,” and “the” may include plural referents unless the context clearly dictates otherwise. Thus, for example, reference to an object may include multiple objects unless the context clearly dictates otherwise.

[00102] As used herein, the terms “substantially,” “substantial,” and “about” are used to describe and account for small variations. When used in conjunction with an event or circumstance, the terms can refer to instances in which the event or circumstance occurs precisely as well as instances in which the event or circumstance occurs to a close approximation. For example, when used in conjunction with a numerical value, the terms can encompass a range of variation of less than or equal to ±10% of that numerical value, such as less than or equal to ±5%, less than or equal to ±4%, less than or equal to ±3%, less than or equal to ±2%, less than or equal to ±1%, less than or equal to ±0.5%, less than or equal to ±0.1%, or less than or equal to ±0.05%.

[00103] Additionally, amounts, ratios, and other numerical values are sometimes presented herein in a range format. It is to be understood that such range format is used for convenience and brevity and should be understood flexibly to include numerical values explicitly specified as limits of a range, but also to include all individual numerical values or sub-ranges encompassed within that range as if each numerical value and sub-range is explicitly specified. For example, a range of about 1 to about 200 should be understood to include the explicitly recited limits of about 1 and about 200, but also to include individual values such as about 2, about 3, and about 4, and sub-ranges such as about 10 to about 50, about 20 to about 100, and so forth.

[00104] While this disclosure has been described with reference to the specific embodiments thereof, it should be understood by those skilled in the art that various changes may be made and equivalents may be substituted without departing from the true spirit and scope of this disclosure as defined by the appended claims. In addition, many modifications may be made to adapt a particular situation, material, composition of matter, method, operation or operations, to the objective, spirit and scope of this disclosure. All such modifications are intended to be within the scope of the claims appended hereto. In particular, while certain methods may have been described with reference to particular operations performed in a particular order, it will be understood that these operations may be combined, sub-divided, or re-ordered to form an equivalent method without departing from the teachings of this disclosure. Accordingly, unless specifically indicated herein, the order and grouping of the operations are not a limitation of this disclosure.

What is claimed is:

1. A battery comprising:

a cathode;

an anode; and

a solid-state electrolyte disposed between the cathode and the anode,

wherein at least one of the cathode, the anode, or the solid-state electrolyte includes a ceramic material including lithium (Li), boron (B), and sulfur (S), the ceramic material includes multiple crystalline phases and has an overall composition given by *a*:*b*:*c* molar ratio of Li:B:S, and *c*/*b* is in a range of about 1 to about 3.

2. The battery of claim 1, wherein *c*/*b* is in a range of about 13/7 to about 3.

3. The battery of claim 1, wherein *c*/*b* is in a range of about 13/7 to about 2.5.

4. The battery of claim 1, wherein *c*/*b* is in a range of about 2.5 to about 3.

5. The battery of claim 1, wherein *a*/*b* is in a range of about 0.5 to about 3.

6. The battery of claim 1, wherein the ceramic material includes at least two different crystalline phases selected from $Li_5B_7S_{13}$, Li_3BS_3, and $Li_2B_2S_5$.

7. The battery of claim 1, wherein the ceramic material includes a first crystalline phase including $Li_5B_7S_{13}$ and a second crystalline phase including $Li_2B_2S_5$.

8. The battery of claim 7, wherein a molar ratio of the first crystalline phase to the second crystalline phase is in a range of about 0.1 to about 10.

9. The battery of claim 1, wherein the ceramic material includes a first phase including $Li_2B_2S_5$ and a second phase including Li_3BS_3.

10. The battery of claim 9, wherein a molar ratio of the first crystalline phase to the second crystalline phase is in a range of about 0.1 to about 10.

11. A battery comprising:

a cathode;

an anode; and

a solid-state electrolyte disposed between the cathode and the anode,

wherein at least one of the cathode, the anode, or the solid-state electrolyte includes a crystalline material including lithium (Li), boron (B), and sulfur (S), and a molar ratio of S:B is about 1 or greater.

12. The battery of claim 11, wherein the molar ratio of S:B is in a range of about 1 to about 3.

13. The battery of claim 11, wherein the molar ratio of S:B is in a range of about 13/7 to about 2.5.

14. The battery of claim 11, wherein the crystalline material includes Li_3BS_3.

15. A battery comprising:

a first electrode;

a second electrode; and

an electrolyte disposed between the first electrode and the second electrode,

wherein at least one of the first electrode or the second electrode includes an electrode additive including a lithium boron sulfide.

16. The battery of claim 15, wherein the lithium boron sulfide is crystalline.

17. The battery of claim 15, wherein the lithium boron sulfide includes at least one of $Li_5B_7S_{13}$, Li_3BS_3, or $Li_2B_2S_5$.

18. A method comprising:

providing a ceramic material including lithium (Li), boron (B), and sulfur (S), wherein the ceramic material includes multiple crystalline phases and has an overall composition given by a:b:c molar ratio of Li:B:S, and c/b is in a range of about 1 to about 3; and

applying an electrical potential across the ceramic material to transport lithium ions through the ceramic material.

19. The method of claim 18, wherein *c/b* is in a range of about 13/7 to about 2.5.

20. The method of claim 18, wherein *c/b* is in a range of about 2.5 to about 3.

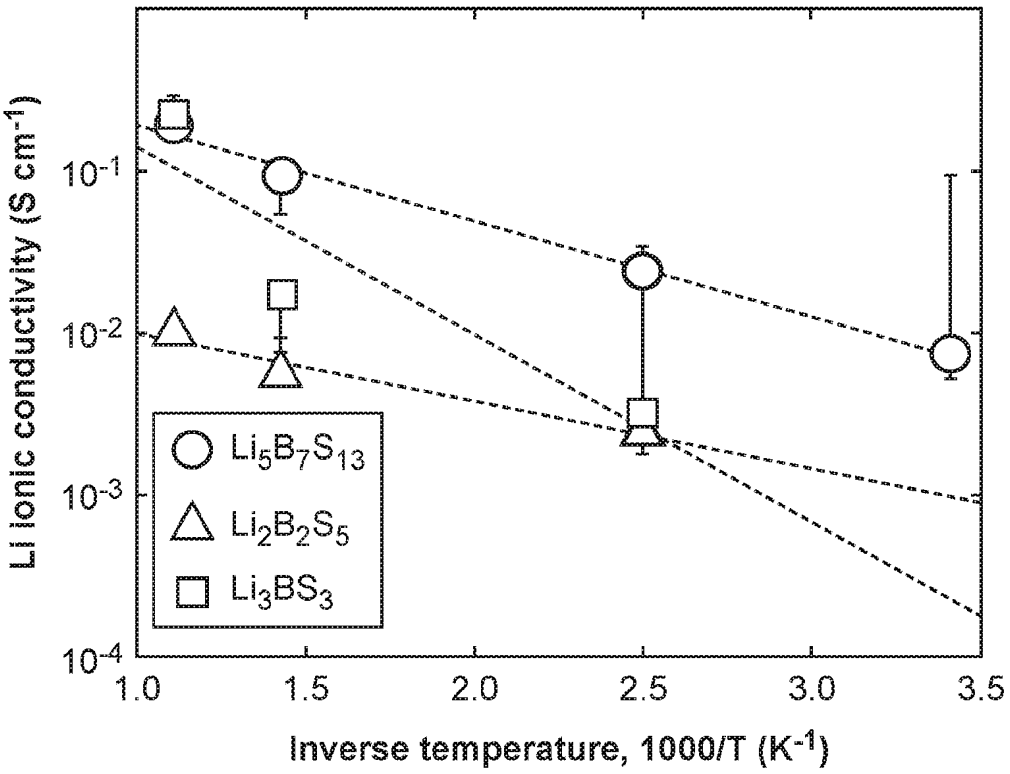
Li ionic conductivity (S cm-1)
10-1
10-2
10-3
10-4
1.0
1.5
2.0
2.5
3.0
3.5
Inverse temperature, 1000/T (K-1)
Li5B7S13
Li2B2S5
Li3BS3

FIG. 1

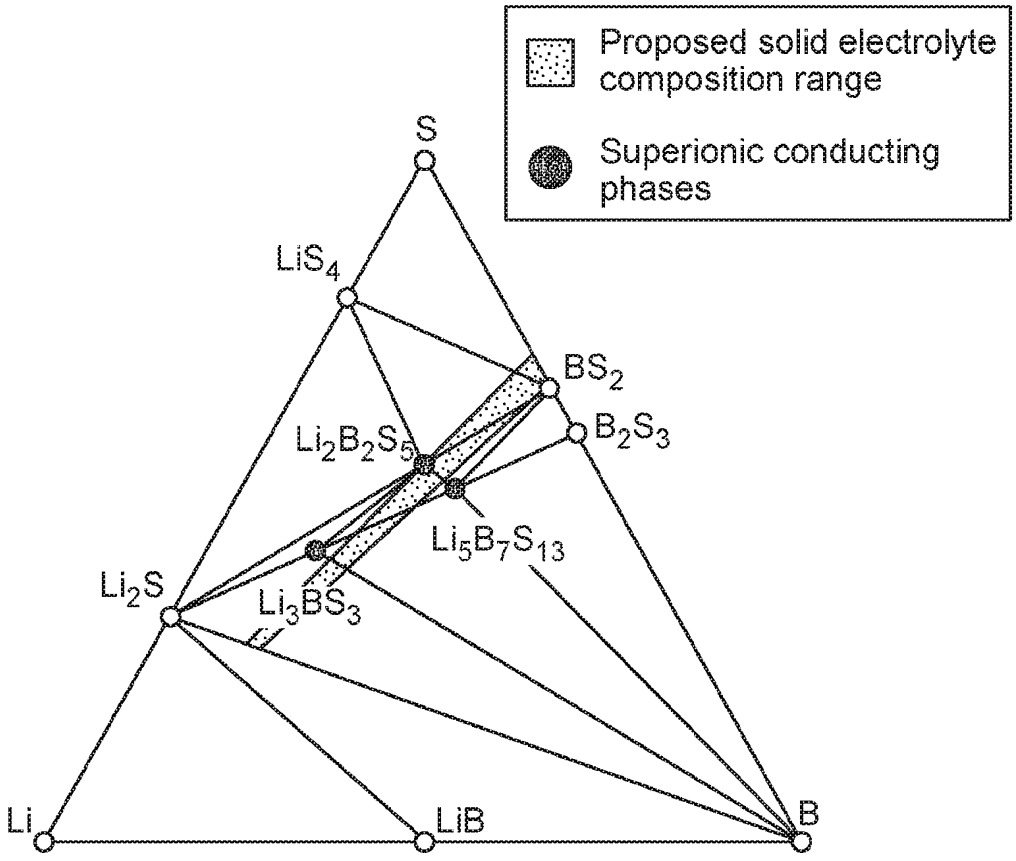
Proposed solid electrolyte composition range
Superionic conducting phases
S
LiS4
BS2
B2S3
Li2B2S5
Li5B7S13
Li2S
Li3BS3
Li
LiB
B

FIG. 2

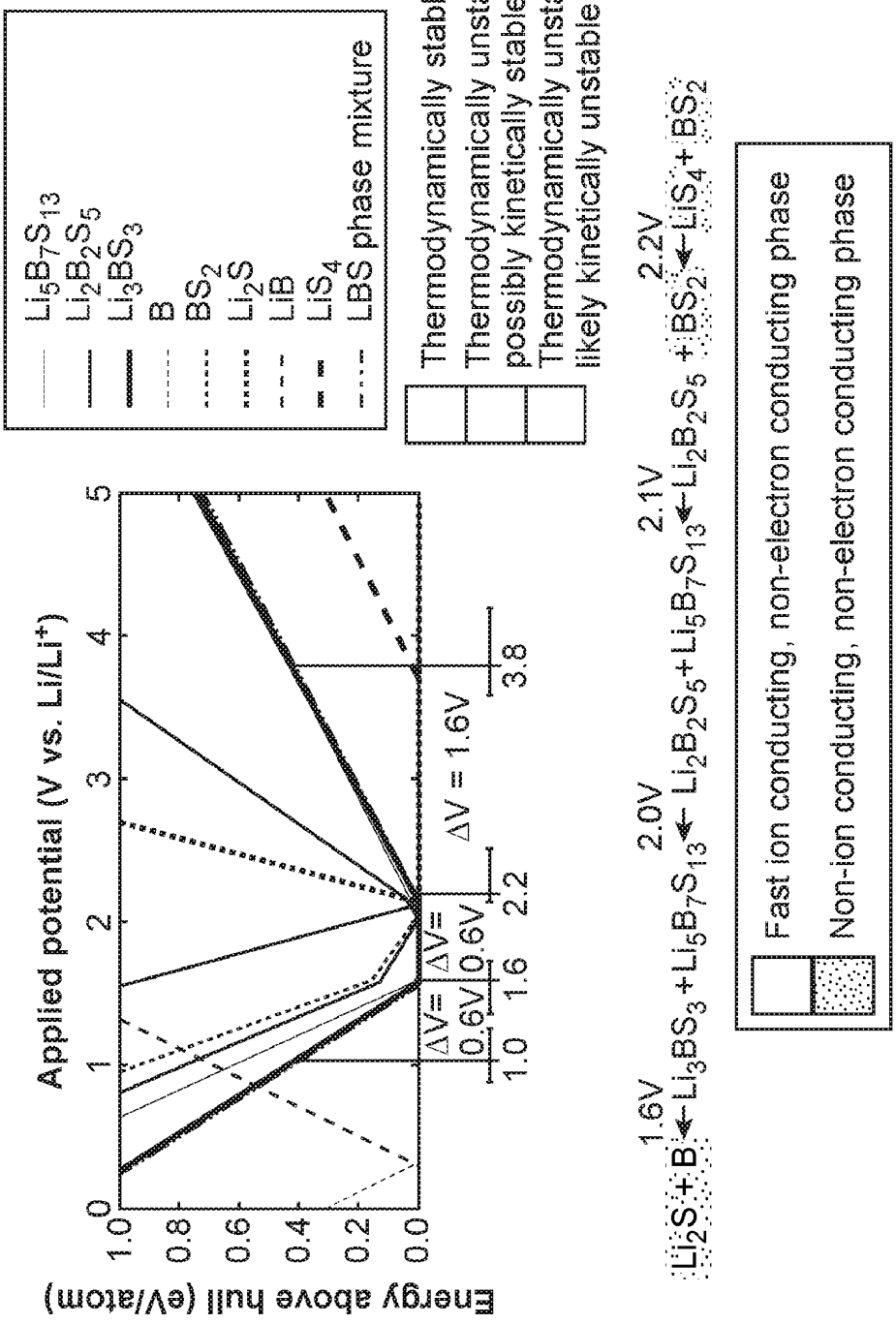
Energy above hull (eV/atom)
Applied potential (V vs. Li/Li+)
0.0
0.2
0.4
0.6
0.8
1.0
0
1
2
3
4
5
ΔV= 0.6V
ΔV= 0.6V
ΔV = 1.6V
1.0
1.6
2.2
3.8
Li5B7S13
Li2B2S5
Li3BS3
B
BS2
Li2S
LiB
LiS4
LBS phase mixture
Thermodynamically stable
Thermodynamically unstable, possibly kinetically stable
Thermodynamically unstable, likely kinetically unstable
1.6V
2.0V
2.1V
2.2V
Li2S + B ← Li3BS3 + Li5B7S13 ← Li2B2S5 + Li5B7S13 ← Li2B2S5 + BS2 ← LiS4 + BS2
Fast ion conducting, non-electron conducting phase
Non-ion conducting, non-electron conducting phase

FIG. 3

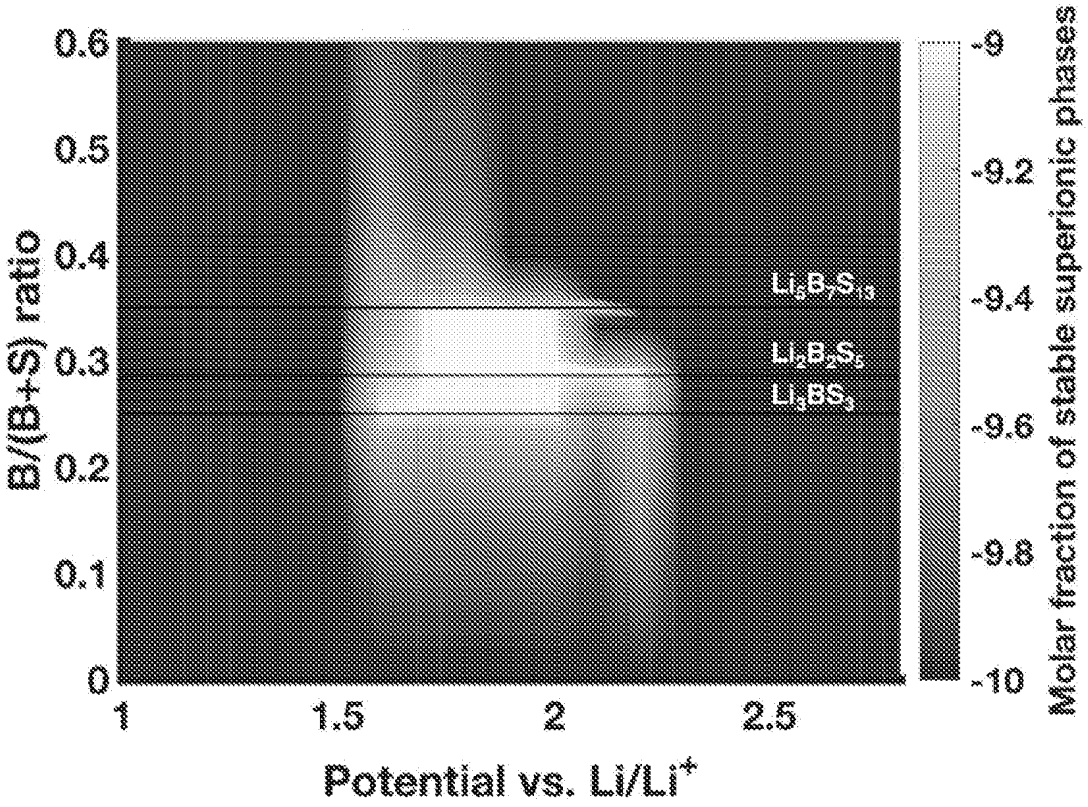
B/(B+S) ratio
0.6
0.5
0.4
0.3
0.2
0.1
0
1
1.5
2
2.5
Potential vs. Li/Li+
Li6B7S13
Li2B2S5
Li3BS3
-9
-9.2
-9.4
-9.6
-9.8
-10
Molar fraction of stable superionic phases

Figure 4

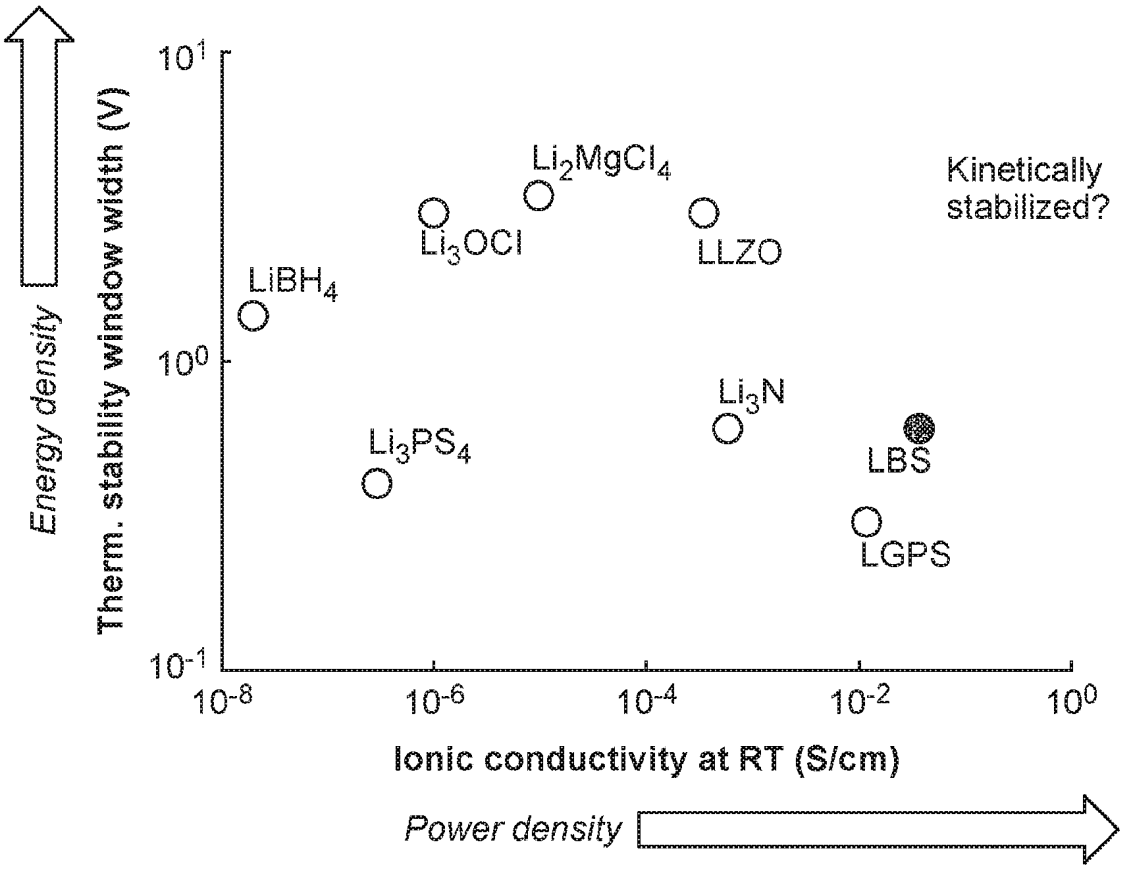
Energy density
Therm. stability window width (V)
10^1
10^0
10^{-1}
Li_2MgCl_4
Kinetically stabilized?
Li_3OCl
LLZO
$LiBH_4$
Li_3N
Li_3PS_4
LBS
LGPS
10^{-8}
10^{-6}
10^{-4}
10^{-2}
10^0
Ionic conductivity at RT (S/cm)
Power density

FIG. 5

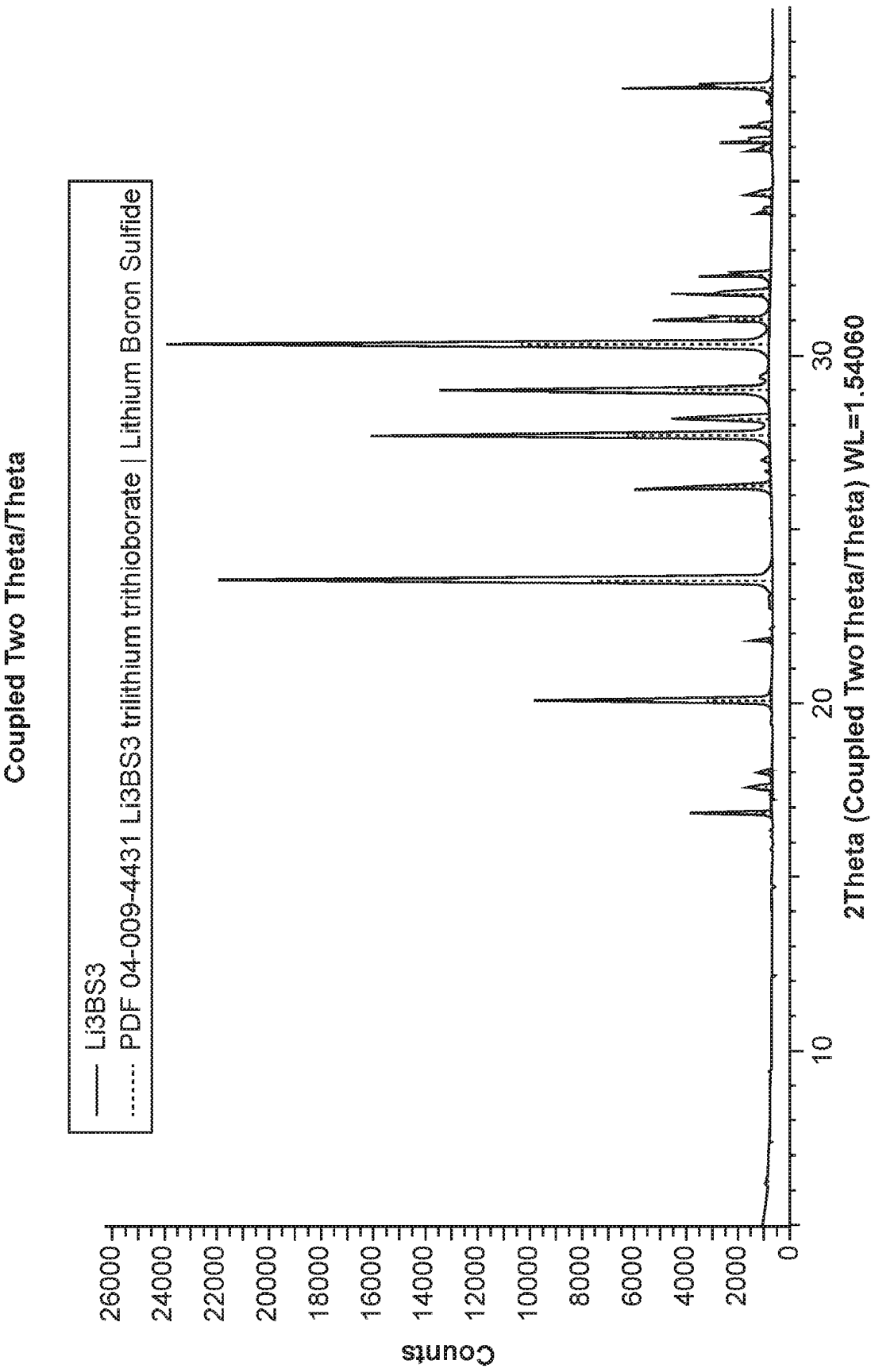
Coupled Two Theta/Theta
Li3BS3
PDF 04-009-4431 Li3BS3 trilithium trithioborate | Lithium Boron Sulfide
Counts
26000
24000
22000
20000
18000
16000
14000
12000
10000
8000
6000
4000
2000
0
10
20
30
2Theta (Coupled TwoTheta/Theta) WL=1.54060

FIG. 6

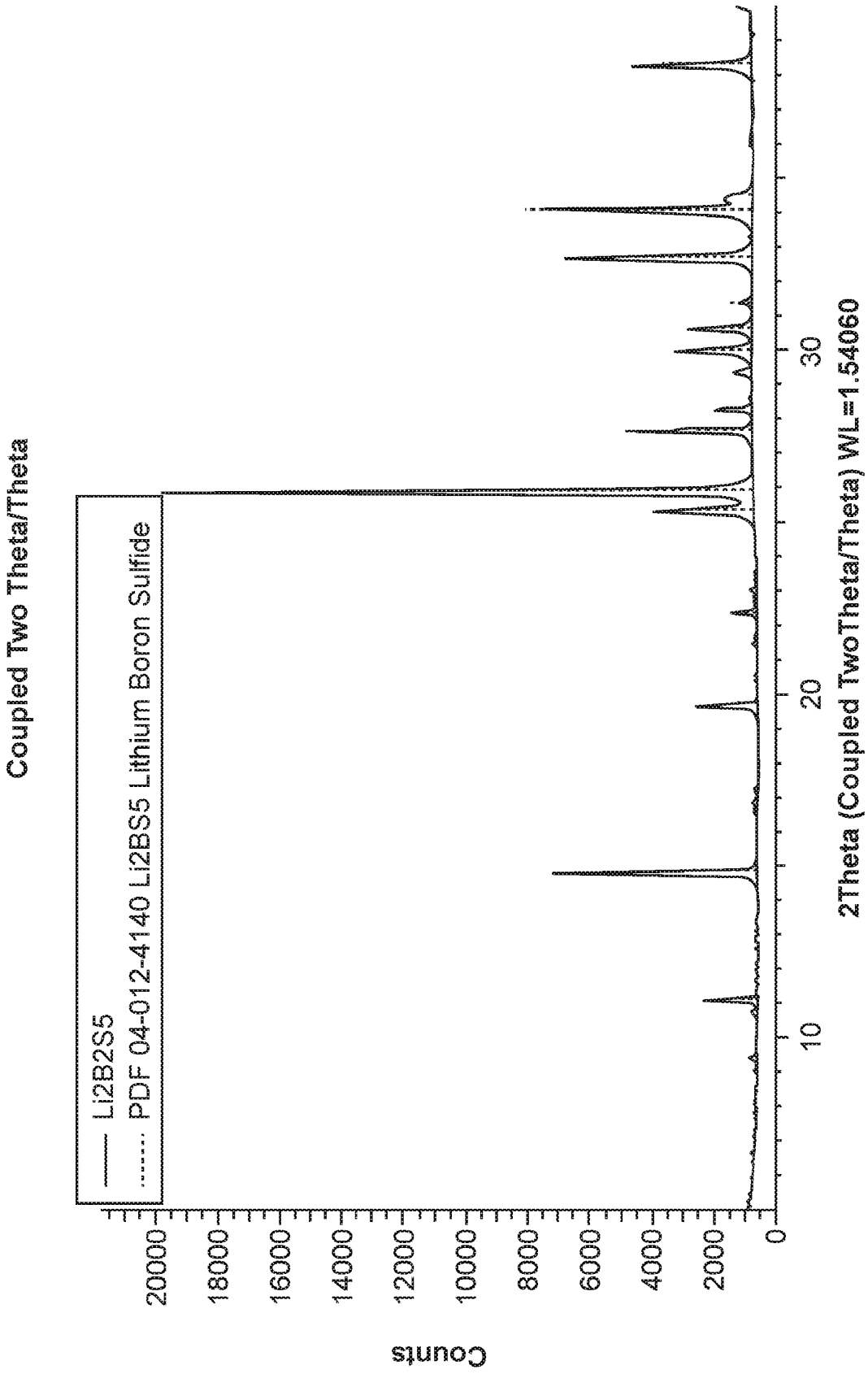
Coupled Two Theta/Theta
Li2B2S5
PDF 04-012-4140 Li2BS5 Lithium Boron Sulfide
Counts
20000
18000
16000
14000
12000
10000
8000
6000
4000
2000
0
10
20
30
2Theta (Coupled TwoTheta/Theta) WL=1.54060

FIG. 7

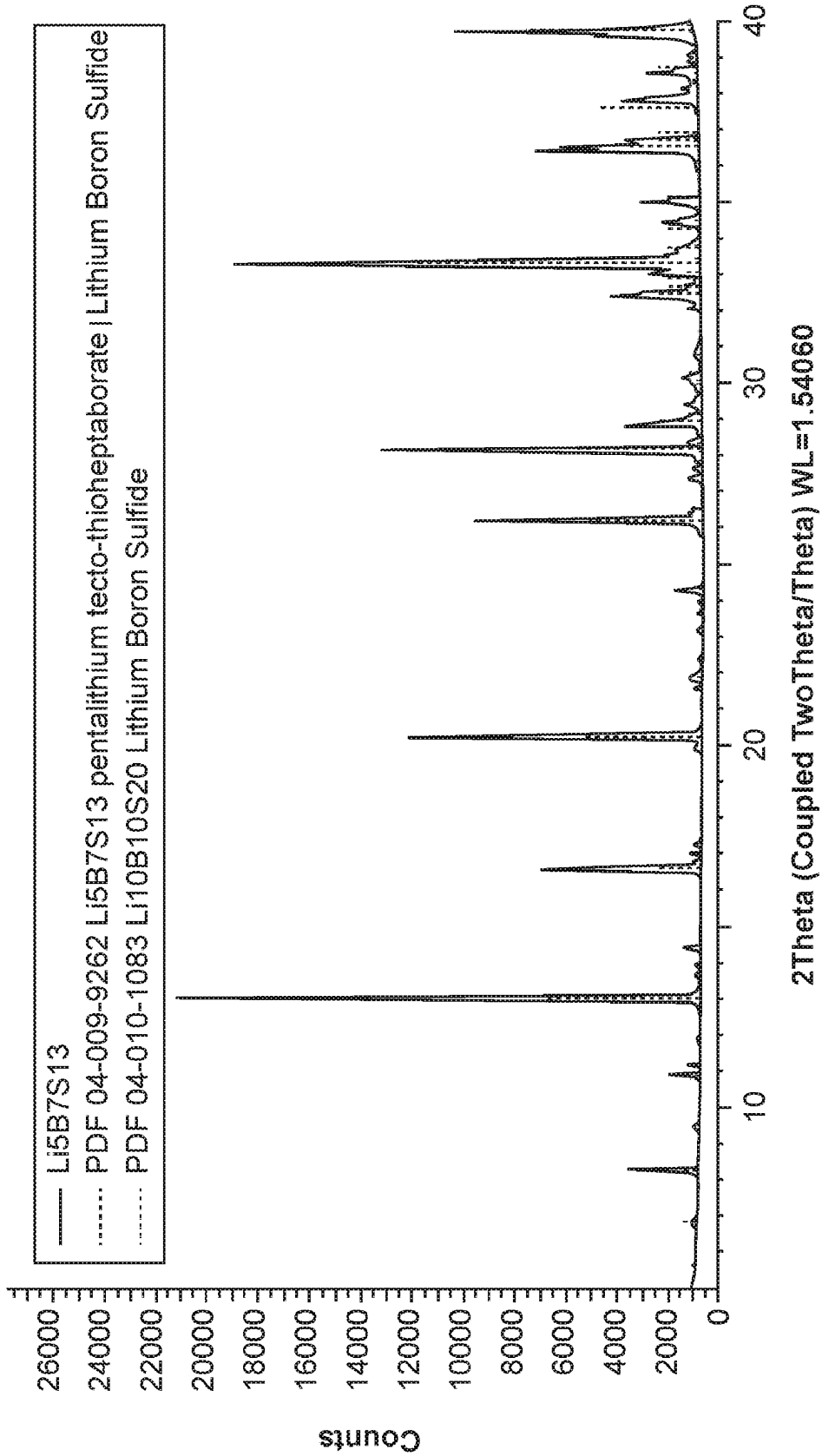
Coupled Two Theta/Theta
Li5B7S13
PDF 04-009-9262 Li5B7S13 pentalithium tecto-thioheptaborate | Lithium Boron Sulfide
PDF 04-010-1083 Li10B10S20 Lithium Boron Sulfide
Counts
26000
24000
22000
20000
18000
16000
14000
12000
10000
8000
6000
4000
2000
0
10
20
30
40
2Theta (Coupled TwoTheta/Theta) WL=1.54060

FIG. 8

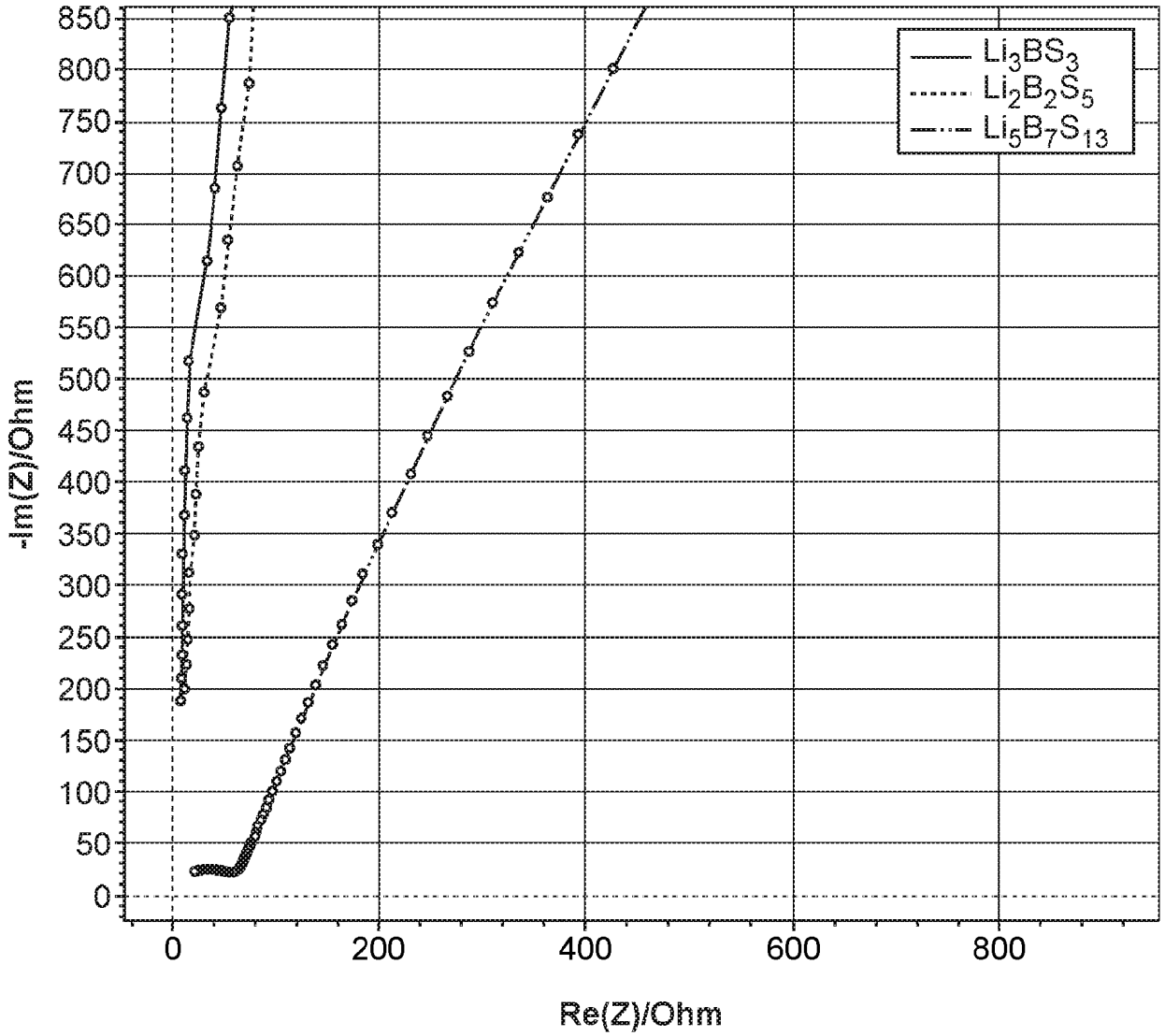
-Im(Z)/Ohm
Re(Z)/Ohm
0
50
100
150
200
250
300
350
400
450
500
550
600
650
700
750
800
850
0
200
400
600
800
Li3BS3
Li2B2S5
Li5B7S13

FIG. 9A

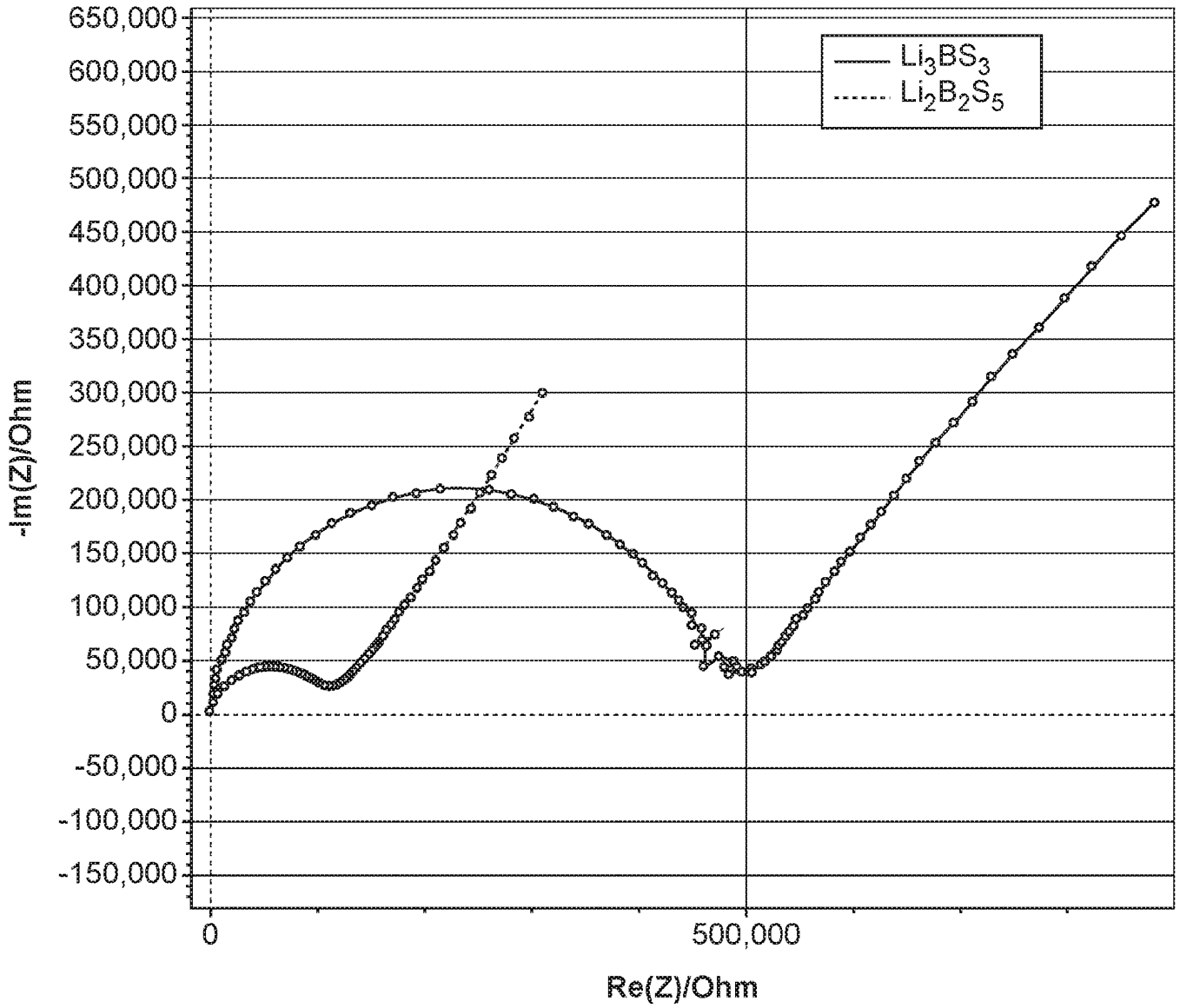
650,000
600,000
550,000
500,000
450,000
400,000
350,000
300,000
250,000
200,000
150,000
100,000
50,000
0
-50,000
-100,000
-150,000
-Im(Z)/Ohm
0
500,000
Re(Z)/Ohm
Li3BS3
Li2B2S5

FIG. 9B

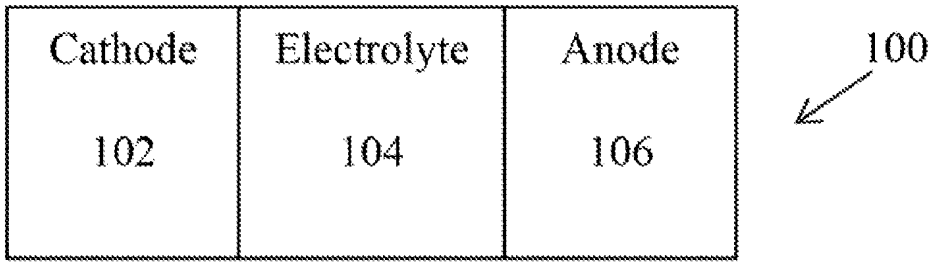

Figure 10

INTERNATIONAL SEARCH REPORT

International application No.
PCT/US2018/050069

A. CLASSIFICATION OF SUBJECT MATTER

H01M 10/0562(2010.01)i, H01M 10/052(2010.01)i

According to International Patent Classification (IPC) or to both national classification and IPC

B. FIELDS SEARCHED

Minimum documentation searched (classification system followed by classification symbols)
H01M 10/0562; H01B 13/00; H01M 10/0525; H01M 10/0585

Documentation searched other than minimum documentation to the extent that such documents are included in the fields searched
Korean utility models and applications for utility models
Japanese utility models and applications for utility models

Electronic data base consulted during the international search (name of data base and, where practicable, search terms used)
eKOMPASS(KIPO internal) & keywords: lithium, boron, sulfur, ceramic material, high lithium ion conductivity

C. DOCUMENTS CONSIDERED TO BE RELEVANT

Category*	Citation of document, with indication, where appropriate, of the relevant passages	Relevant to claim No.
X	US 2015-0357675 A1 (TOYOTA JIDOSHA KABUSHIKI KAISHA) 10 December 2015 See claim 1; and paragraphs [0017], [0018], [0040], [0045], [0046].	11,12,14-17
Y		13
A		1-10,18-20
Y	SENDEK, A. D. et al., "Holistic computational structure screening of more than 12000 candidates for solid lithium-ion conductor materials", Energy & Environmental Science, 2017 (E-pub. 2016.12.01), Vol. 10, No. 1, pp. 306-320 See abstract; 1. Introduction section; and table 3.	13
X	US 2015-0349377 A1 (SUGIURA, K. et al.) 03 December 2015 See claims 1, 4, 9-11; and paragraphs [0032], [0033], [0043].	11,12,14-17
A	US 2015-0340734 A1 (FUJITSU LIMITED) 26 November 2015 See claims 1, 2, 4, 7, 8, 12.	1-20
A	JP 2013-232418 A (IDEMITSU KOSAN CO., LTD.) 14 November 2013 See claims 1-19.	1-20

☒ Further documents are listed in the continuation of Box C. ☒ See patent family annex.

* Special categories of cited documents:
"A" document defining the general state of the art which is not considered to be of particular relevance
"E" earlier application or patent but published on or after the international filing date
"L" document which may throw doubts on priority claim(s) or which is cited to establish the publication date of another citation or other special reason (as specified)
"O" document referring to an oral disclosure, use, exhibition or other means
"P" document published prior to the international filing date but later than the priority date claimed
"T" later document published after the international filing date or priority date and not in conflict with the application but cited to understand the principle or theory underlying the invention
"X" document of particular relevance; the claimed invention cannot be considered novel or cannot be considered to involve an inventive step when the document is taken alone
"Y" document of particular relevance; the claimed invention cannot be considered to involve an inventive step when the document is combined with one or more other such documents,such combination being obvious to a person skilled in the art
"&" document member of the same patent family

Date of the actual completion of the international search	Date of mailing of the international search report
24 December 2018 (24.12.2018)	**24 December 2018 (24.12.2018)**

Name and mailing address of the ISA/KR
International Application Division
Korean Intellectual Property Office
189 Cheongsa-ro, Seo-gu, Daejeon, 35208, Republic of Korea
Facsimile No. +82-42-481-8578

Authorized officer
LEE, Ki Cheul
Telephone No. +82-42-481-3353

INTERNATIONAL SEARCH REPORT

International application No.
PCT/US2018/050069

C (Continuation). DOCUMENTS CONSIDERED TO BE RELEVANT

Category*	Citation of document, with indication, where appropriate, of the relevant passages	Relevant to claim No.
PX	BIANCHINI, F. et al, "A first-principle investigation of the Li diffusion mechanism in the super-ionic conductor lithium orthothioborate Li3BS3 structure", Materials Letters, 2018 (E-pub. 2018.02.21.), Vol. 219, pp. 186-189 See abstract; 1. Introduction section; 3. Results and discussion section; and 4. Conclusions section.	11,12,14-17

INTERNATIONAL SEARCH REPORT

Information on patent family members

International application No.

PCT/US2018/050069

Patent document cited in search report	Publication date	Patent family member(s)	Publication date
US 2015-0357675 A1	10/12/2015	AU 2014-280008 A1	23/01/2014
		AU 2014-280008 B2	29/10/2015
		CA 2840671 A1	10/01/2013
		CN 103650231 A	19/03/2014
		CN 103650231 B	25/11/2015
		EP 2712468 A1	02/04/2014
		JP 2013-016423 A	24/01/2013
		JP 5443445 B2	19/03/2014
		KR 10-1506109 B1	25/03/2015
		KR 10-2014-0025542 A	04/03/2014
		US 2014-0141341 A1	22/05/2014
		US 9172113 B2	27/10/2015
		US 9484597 B2	01/11/2016
		WO 2013-005085 A1	10/01/2013
US 2015-0349377 A1	03/12/2015	AU 2013-369026 A1	03/07/2014
		AU 2013-369026 B2	21/07/2016
		BR 112015015726 A2	11/07/2017
		CA 2896704 A1	03/07/2014
		CA 2896704 C	23/05/2017
		CN 105050976 A	11/11/2015
		CN 105050976 B	16/06/2017
		EP 2938583 A1	04/11/2015
		EP 2938583 B1	30/11/2016
		JP 2014-127388 A	07/07/2014
		JP 5757284 B2	29/07/2015
		KR 10-1708579 B1	20/02/2017
		KR 10-2015-0088849 A	03/08/2015
		TW 201442977 A	16/11/2014
		TW I500589 B	21/09/2015
		WO 2014-102580 A1	03/07/2014
US 2015-0340734 A1	26/11/2015	CN 104995691 A	21/10/2015
		CN 104995691 B	25/07/2017
		EP 2958111 A1	23/12/2015
		EP 2958111 B1	14/02/2018
		JP 6070815 B2	01/02/2017
		WO 2014-125633 A1	21/08/2014
JP 2013-232418 A	14/11/2013	CN 101821894 A	01/09/2010
		CN 101821894 B	19/12/2012
		EP 2211415 A1	28/07/2010
		EP 2211415 B1	06/11/2013
		JP 5270563 B2	21/08/2013
		JP 5577425 B2	20/08/2014
		KR 10-1442306 B1	22/09/2014
		KR 10-2010-0081296 A	14/07/2010
		TW 200923972 A	01/06/2009
		TW I464750 B	11/12/2014

INTERNATIONAL SEARCH REPORT

Information on patent family members

International application No.

PCT/US2018/050069

Patent document cited in search report	Publication date	Patent family member(s)	Publication date
		US 2010-0200795 A1	12/08/2010
		US 8518585 B2	27/08/2013
		WO 2009-047977 A1	16/04/2009